Chapter 3: Supported Nickel Metal-Based Catalysts

Ashutosh Kumar et.al. [1] and Meng Ni et.al. [2] have reviewed reforming of Bioethanol. They have covered both noble and non-noble metal catalysts. They report that Rh and Ni are the best active metals for this reaction. Between the two Ni is significantly cheaper and more economical to use. Meng Ni et.al. state that both Rh and Ni are not active for the water gas shift reaction (WGSR) which is important for enhancing yield of H_2. They recommend use of alloys or tandem catalyst for the same. However, it is noted from the results of the current study (chapters 4 and 5) that the WGSR is promoted by the choice of support in the case of Ni catalysts. The literature reviewed by them mostly covers mono-component supports. Contreras et.al [3] have also carried out an exhaustive review of catalysts for ethanol steam reforming. They have reviewed active metals as well as support components and listed those that show promise. They infer that impregnation as a method of preparation produces the best catalysts. They have provided comments connecting catalyst composition and characteristics to performance. These cover properties such as hydrothermal stability, acidity, metal dispersion, oxygen content of support, metal support interaction, XRD phase of support components such as perovskites, spinels or solid solution and metal reducibility. They conclude that Rh, Ru, Pd and Ir (amongst noble metals) followed by Ni, Co and Cu (amongst non-noble metals) show high selectivity to H_2. Amongst supports they cite Al_2O_3, TiO_2, MgO, Ceria-zirconia, alkaline earth-ceria-zirconia, lanthanum oxycarbonate and alumina-zirconia as promising. The catalysts reviewed by them mostly constitute mono and bi-component supports. It is also noted that these components are reported to impart specific properties to the catalyst, for example, basic components such as MgO decrease acidity and thus minimize formation of ethylene by dehydration, ceria imparts lattice oxygen which is considered favorable for scavenging coke deposits and thus improving catalyst life, lanthana imparts thermal stability, zirconia imparts hydrothermal stability etc. Thus, a good catalyst with commercial potential needs to have multiple properties and hence necessarily needs to be multi-component. The data available in literature does not provide information about how properties of individual components are affected due to interaction between them in multi-component catalysts. Determining this requires a systematic study at monocomponent, bicomponent and multi-components levels of the same set of components. The current work addresses this gap in literature.

Based on the inferences drawn from the above reviews a set of seventeen catalysts were prepared by impregnating Nickel on binary (alumina or magnesia or zirconia along with rare earth), ternary supports (combinations of Al-Zr, Al-Mg or Mg-Zr along with rare earth) and quaternary supports (combinations of all three alumina, magnesia and zirconia along with rare earth component). The supports contained nominal 5.4 wt% each of lanthana and ceria. The composition of alumina, magnesia and zirconia were varied in the ternary and quaternary supports. The nickel content was maintained at 7.5 wt% for all thirteen supports. In addition, Nickel content was decreased to 5wt% and increased to 10wt% for two ternary supports, one each of alumina-magnesia and alumina-zirconia. These latter supports contained equal concentrations by weight of alumina and magnesia or alumina and zirconia. The catalysts were calcined at 550^{o}C. They were characterized by Nitrogen (N_2) physisorption for microstructure, pulse chemisorption for dispersion of nickel, Ammonia Temperature Programmed Desorption (NH_3-TPD) for acidity, X-ray Diffractometry (XRD) for Phase and Crystallite Size, Temperature Programmed Reduction (TPR) for metal reducibility and Transmission Electron Spectroscopy (TEM) for nickel cluster size. These catalysts were evaluated to correlate their properties with the performance of the Steam Reforming of Ethanol reaction (presented in Chapter 4) and the Dry Reforming of Ethanol reaction (presented in Chapter 5) for hydrogen generation through syngas.

3.1: Preparation of supported Ni catalysts

Catalysts were prepared by incipient technique also known as dry impregnation technique. The advantage of this technique is that it does not generate waste liquid streams for disposal. First, the water pickup capacity of the carriers is determined by soaking a known weight of the carrier in water. Excess water is decanted and the increase in weight is determined. Water pick-up is derived using the below-mentioned formula.

Water pickup capacity (wt%) = 100 x (weight gained by the carrier/initial weight of the carrier).

Loss on ignition (LOI) is also determined by holding the carrier at 550 ^{o}C for a duration of 1 hour and determining the loss in weight. This is repeated till the weight loss was constant.

LOI (%) = 100 x (change in weight of carrier/initial weight of the carrier).

The LOI is taken into consideration for deciding the quantity of Nickel salt to be used for impregnation.

An aqueous solution of Nickel Nitrate is prepared by dissolving the required quantity of Nickel Nitrate Hexahydrate salt (Sigma Aldrich make, CAS Number: 13478-00-7) in demineralized water (DM water). The quantity of DM Water corresponds to the water pick-up capacity of that carrier. The Nickel content of the solution corresponds to the quantity required to achieve Nickel concentration in the final catalyst on LOI free basis. The Nickel salt solution is sprayed onto the carrier in a rotating drum mixer. The catalyst is rotated for 15 minutes till it is free-flowing. It is then aged overnight at ambient temperature for proper distribution of the active phase. It is further dried at 120^{o}C for 8 hours in an air oven and calcined at 550^{o}C for 4 hours in a furnace in the atmospheric environment. Wang et.al [16] have studied monolayer capacity of NiO deposited as Ni nitrate and Ni acetate by impregnation on γ-Al_2O_3. They conclude that the former yields higher dispersion capacity than the latter and is hence a better choice as a precursor.

3.2: Chemical composition of the catalysts

The chemical composition of the catalysts was determined by Inductively Coupled Plasma Optical Emission spectroscopy (ICP-OES) analysis. A known quantity of the catalyst is dissolved in aqua regia and diluted appropriately. The diluted solution is aspirated into the plasma of the ICP-OES instrument. Quantification is done using a standard solution of the corresponding elements. The chemical composition of the catalysts is presented in Table 2. The nomenclature is the same as that of the supports. Content of Ni is prefixed to the abbreviation of the support.

The standard deviations of lanthana, ceria (at nominal 5.5 wt% each) and Nickel at nominal 7.5 wt% are 0.113, 0.125 and 0.0887 respectively. Thus, the compositions are close to the target.

Table 2: Chemical composition of supported Nickel catalysts

Catalyst	Ni (wt%)	La_2O_3 (wt%)	CeO_2 (wt%)	Al_2O_3 (wt%)	MgO (wt%)	ZrO_2 (wt%)
7.5Ni-AMZ-89-0-0	7.5	4.9	4.8	82.9	0	0
7.5Ni-AMZ-0-89-0	7.4	5.1	4.9	0	82.7	0
7.5Ni-AMZ-0-0-89	7.4	5.1	4.8	0	0	82.7
7.5-NiAMZ-44-44-0	7.6	5.1	5.0	41.3	41.3	0
7.5Ni-AMZ-0-44-44	7.7	4.9	4.9	0	41.3	41.3
7.5Ni-AMZ-44-0-44	7.5	4.9	4.8	41.3	0	41.3
5Ni-AMZ-44-44-0	5.1	5.1	5.1	42.3	42.3	0
10Ni-AMZ-44-44-0	10.2	4.8	4.8	40.2	40.2	0
7.5Ni-AMZ-39-49-0	7.4	5.1	5.0	36.5	46	0
7.5Ni-AMZ-29-59-0	7.5	5.1	5.1	27.5	55	0
7.5Ni-AMZ-39-0-49	7.6	4.9	5.0	36.5	0	46.0
7.5Ni-AMZ-29-0-59	7.5	4.9	5.0	27.5	0	55.0
5Ni-AMZ-44-0-44	5.0	5.1	5.1	42.3	0	42.3
10Ni-AMZ-44-0-44	10.4	4.8	4.8	40.2	0	40.2
7.5Ni-AMZ-44-22-22	7.5	4.9	5.0	41.25	20.6	20.6
7.5Ni-AMZ-22-44-22	7.4	5.0	5.1	20.62	41.3	20.6
7.5Ni-AMZ-22-22-44	7.6	5.0	5.1	20.62	20.6	41.3

3.3: Microstructure of the supported metal catalysts

The BET-specific surface area of the catalysts is shown in Figure 23 below. A Quantachrome QUADRASORB SI IV N_2 physisorption unit was used for measuring BET specific surface area The specific surface area was calculated using the BET (Brunauer-Emmet-Teller) equation. Samples were degassed under vacuum at 300°C using a FloVac instrument for 3 hours before measurement. The BET-specific surface area of the corresponding supports used for preparing these catalysts is also included in Figure 23.

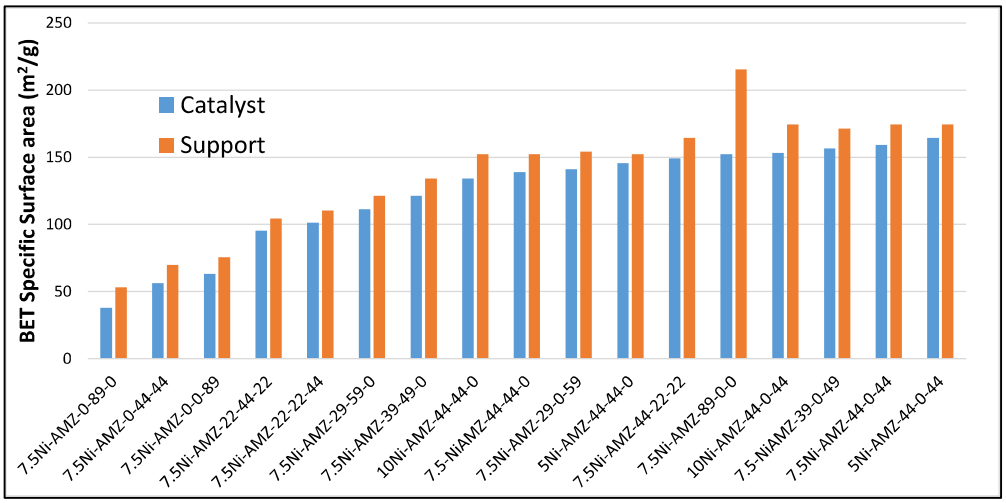

Figure 23: Comparison of BET-specific surface area of the Nickel catalysts and corresponding support

The following inferences can be drawn from the trend in Figure 23:

- Within the catalysts wherein Nickel is supported on binary supports which comprise one of alumina or magnesia or zirconia along with lanthana and ceria at fixed composition, the specific surface area decreases in the order Al>>Zr>Mg. These trends are the same as for the supports used in preparing these catalysts. The catalyst with Ni supported on binary alumina support (AMZ-89-0-0) shows a larger decrease of specific surface area relative to the support than other catalysts. Yaakob et.al. [4] have studied catalysts which constitute 5% Ni impregnated on Alumina prepared by sol-gel method. They report specific surface area 292 m^2/g against 215 m^2/g achieved in the current work. Thus, sol gel results in higher surface area. However, it is an expensive method of preparation involving organic solvents. Frusteri et.al. [5] have studied Ni supported on MgO. They report specific surface area 45 m^2/g which is comparable to the value obtained for AMZ-0-89-0 in the current study. Biswas et.al. [6] have studied 10-40 wt% Nickel supported on CeO_2, ZrO_2 and mixed oxides of ceria and zirconia with CeO_2/ZrO_2 weight ratio varying from 0.25-4. The supports are prepared by co-precipitation and Nickel is impregnated by incipient wetness. They report BET specific surface area of 24.5 m^2/g for the ZrO_2-supported catalyst. Similarly, Shuirong Li et.al [7] have reported specific surface area 91 m^2/g for 15% Ni supported on ZrO_2 prepared by gelation and 40 m^2/g for catalyst prepared by conventional precipitation

route. The binary AMZ-0-0-89 sample of the present study shows a surface area of 63 m^2/g for Ni content of 7.5 wt% which is higher than that reported by Biswas et.al. and lower than that of Li et.al. A possible reason for this trend is the difference in Nickel content of the catalysts prepared in the current study. Seung Han et.al. [8] have studied 10%Ni-Al_2O_3-ZrO_2 xerogel catalysts with different Zr/Al mole ratios (0-0.4), which are prepared by single-step epoxide driven sol-gel method. They report a decrease in specific surface area with increasing Zr content which is attributed to lattice contraction of ZrO_2 due to the incorporation of Al^{3+}. A similar trend of decrease in the surface area of the ternary Al-Zr support with increasing zirconia content is also observed in the current study (Figure 23 above).

- Within the catalysts wherein Nickel is supported on Ternary supports, the trend again remains the same as that of the supports. Specific surface area decreases in the order Alumina-zirconia > alumina-magnesia > magnesia-zirconia. Galetti et.al [9] have studied magnesium aluminate supports promoted by rare earth (5 wt%) with 8 wt% Nickel for the steam reforming of ethanol. The catalysts are prepared by the citrate method wherein stoichiometric quantities of nitrates of Alumina and Magnesium are mixed with citric acid followed by evaporation to dryness and calcination in N_2 at 500°C (2 hours) and in air at 700°C (4 hours). Rare earth Ce or Pr are incorporated by impregnation using their acetates. Ni is impregnated using nitrate or acetate. The BET-specific surface area reported by these authors for the magnesium aluminate support is 60 m^2/g and for the catalysts, it is 39-36 m^2/g. The supports of the current study have stoichiometric excess of magnesium, and although MgO alone (0-89-0) has a surface area of 38 m^2/g, the ternary Al_2O_3-MgO catalysts have a surface area ranging from 111 – 139 m^2/g which is significantly larger than that reported by Galetti et. al [9]. Thus, co-precipitation has an advantage over the citrate method.
- Within the catalysts wherein Nickel is supported on quaternary supports, the trend is similar to that of binary catalysts. The catalyst with the highest alumina content in its carrier shows the highest specific surface area followed by the catalyst with the highest zirconia content and then the highest magnesia content.
- Overall, alumina serves to significantly increase the specific surface area of both the ternary catalysts which contain magnesia or zirconia.

- Between the series the binary catalysts of magnesia or zirconia show amongst the lowest specific surface area. Likewise, the ternary catalyst of magnesia-zirconia. Skewed catalysts of alumina-zirconia follow. The quaternary catalysts that are rich in magnesia or zirconia also show significantly lower specific surface area. Ternary alumina-magnesia catalysts with balanced composition or binary alumina, quaternary catalyst rich in alumina and ternary alumina-zirconia with balanced composition show specific surface areas on the higher side with small differences between them. Ternary alumina-zirconia catalysts with balanced composition and the catalysts with skewed composition with lower zirconia (AMZ-39-0-49) show amongst the highest specific surface area.

The trend of change in BET specific surface area of the catalyst with Nickel content for a given support is shown in Figure 24 below. The two supports used in the study are ternary supports of alumina and magnesia and alumina and zirconia.

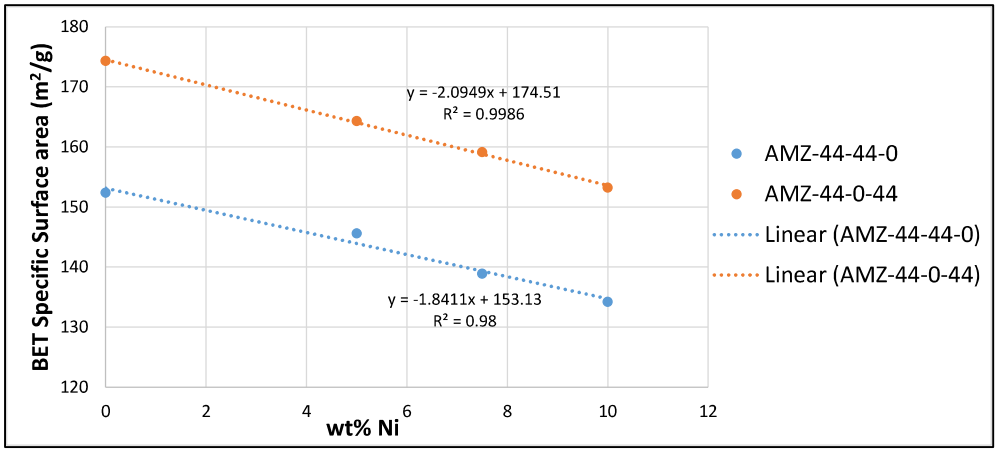

Figure 24: Change in BET-specific surface area with Nickel content of the catalyst.

As seen from Figure 24, the BET-specific surface area shows a linear trend with Nickel content varying from 5 to 10 wt%. It decreases between 1.8 to 2.1 m^2/g per wt% Nickel. It is to be noted that the Nickel is in the form of its oxide in the catalysts. The change per unit weight of NiO is similar for both the catalysts although the starting specific surface area of the supports differs by 22 m^2/g.

Navarro et.al [10] have studied M_xO_y-Al_2O_3 catalysts, where M= Zr, Ce, La or Mg, M/Al 0.035 (atomic), are impregnated onto an alumina support (Alfa Aesar) with specific surface area 212 m^2/g. The catalysts are calcined at 550 °C-650°C. Further, 16-17 wt% NiO is impregnated onto these supports followed by calcination at 500°C. Their

results show a decrease in the surface area of the carrier ranging from nil to 5 m^2/g with practically no change in pore volume. This result is contrary to the results of the current study. It is also surprising because the deposition of 16-17 wt% Nickel is expected to result in some pore blockage and hence loss of surface area and pore volume.

The pore volumes of the catalysts along with the pore volume of the support used to prepare them are shown in Figure 25 below.

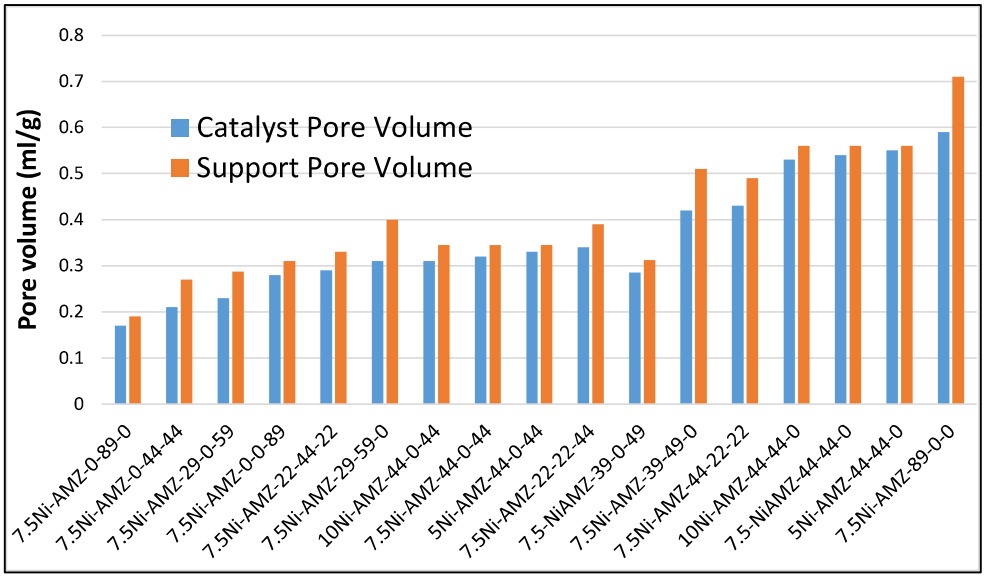

Figure 25: Pore volumes of supported Nickel metal-based catalysts.

As seen from the trend in Figure 25, the specific pore volume of the catalysts is slightly lower than that of the supports used to prepare them in all the cases. This is consistent with the expectation of some loss of pore volume upon impregnating NiO onto the support.

The pore volume of the binary catalysts decreases in the order Al >> Zr > Mg>. This is similar to the trend of the specific surface area of these catalysts.

The trend of ternary catalysts is AMZ-44-44-0>AMZ-39-49-0>AMZ-39-0-49>AMZ-44-0-44>AMZ-29-59-0>AMZ-29-0-59>AMZ-0-44-44. Thus, ternary catalysts with balanced Al-Mg show the highest pore volume followed by ternary catalysts of the skewed composition of alumina-magnesia or alumina-zirconia but with the magnesia or zirconia at a relatively lower value. This is followed by catalysts with balanced alumina-zirconia composition, catalysts of a skewed composition of alumina-magnesia or alumina-zirconia but with the magnesia or zirconia at a relatively higher

value, and finally catalysts with a balanced composition of magnesia-zirconia. This trend is different from that of the specific surface area.

The quaternary catalysts show pore volume decreasing in the order Al>Zr>Mg which is similar to that of the binary catalysts. The trend is also similar to that of the specific surface area of these catalysts.

The trend of change in specific pore volume of the catalyst with Nickel content for a given support is shown in Figure 26 below. The two supports used in the study are ternary supports of alumina and magnesia and alumina and zirconia.

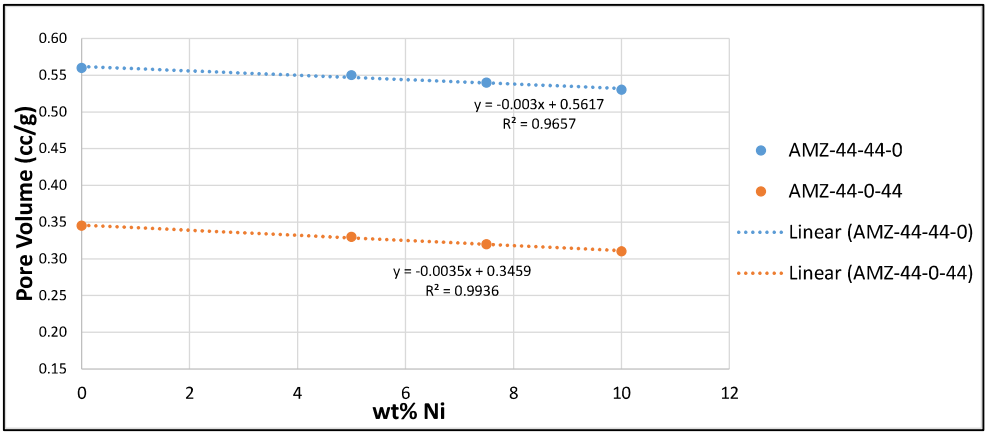

Figure 26: Change in the specific pore volume of the catalysts with Nickel content of the catalyst.

As seen in Figure 26, the specific pore volume decreases by 0.003 ml/g per wt% Nickel loading in the support. The value holds good for both the ternary supports. It is to be noted that the Nickel is in the form of its oxide in the catalysts.

3.4: Acidity of the catalysts by NH_3 TPD

The acidity of the catalysts is determined by NH_3 TPD studies. A Micromeritics Autochem-2920 instrument was used for this purpose. Samples are first heated in a flow of carrier gas to 500°C to remove adsorbed substances. They are then cooled to 50°C and saturated with a flow of NH_3 in Helium at 50°C. A calibration gas mixture with composition 5 vol% NH_3 in Helium is used for this purpose. The flow rate is 50 ml/min for a duration of 30 minutes. The samples are then flushed for 1 hour with a flow of 10 ml/min Helium to desorb weakly adsorbed NH_3. The TPD is recorded by ramping the temperature from 50°C to 900°C at 10°C/min in a flow of He. Profiles of NH_3 desorption as a function of temperature are shown in Appendix 6.

All the catalysts show two desorption peaks. The peak at a lower temperature (93°C to 115°C) corresponds to weakly adsorbed ammonia whereas the peak at a higher temperature (213°C to 260°C) corresponds to strongly adsorbed ammonia representing weak and strong acidity respectively. Strong acidity is generally regarded as important for catalysis.

The trend of strong acidity of the catalysts is compared between themselves and also with the corresponding support in Figure 27 below. Catalysts, wherein Nickel content is varied, are coded in the same color (yellow for AMZ-44-0-44 and green for AMZ-44-44-0).

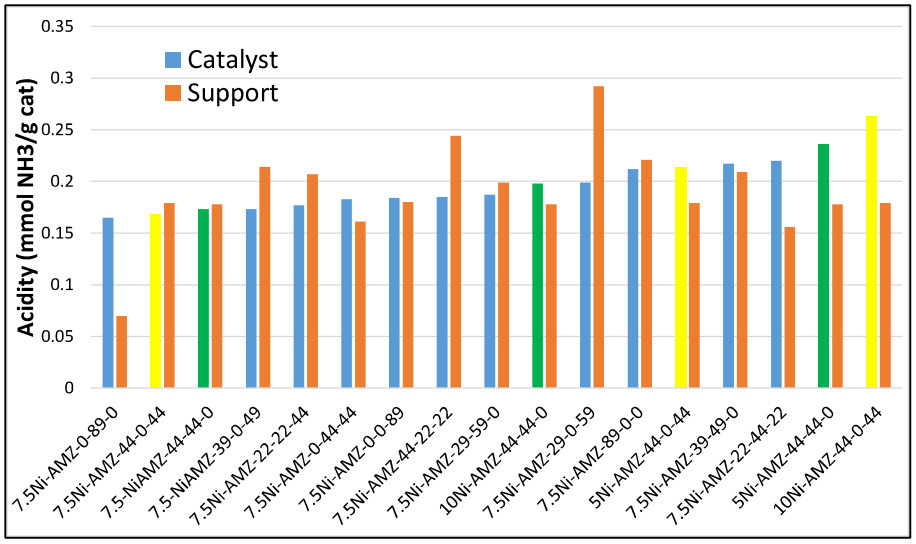

Figure 27: Trend of strong acidity of the catalysts and the corresponding supports used to prepare them.

As seen from the trend in Figure 27, the binary catalysts show the trend of strong acidity of alumina-based catalyst > zirconia based > Magnesia based. This is in line with the strong acidity of the supports. However, while the alumina and zirconia-based binary catalysts show acidity values similar to that of the support, the magnesia-containing catalyst (7.5Ni-AMZ-0-89-0) shows a significant increase in acidity. This increase in acidity is attributed to Lewis acidity resulting from NiO as suggested by Yang et.al. [11].

The strong acidity of the catalysts increases with increasing zirconia content in ternary Al-Zr catalysts. Such a trend is not evident with the MgO content of the ternary Al-Mg catalysts. Seung Han et.al. [8] have studied 10%Ni-Al_2O_3-ZrO_2 xerogel catalysts with different Zr/Al mole ratios (0-0.4), which are prepared by single-step

epoxide driven sol-gel method. They report that acidity decreases with increasing zirconia content which is contrary to the results of the current study. Differences in the formation of zirconia-alumina solid solution could be a possible reason for this.

The trend of strong acidity with Nickel content of the catalyst is 5%Ni > 10% > 7.5% for the catalyst AMZ-44-44-0 whereas it shows a trend of 10% Ni> 5% >7.5% for the catalyst series AMZ-44-0-44. While both catalysts with 7.5% show the lowest strong acidity in both series, the trend of catalysts containing 5 and 10% Nickel reverses in these supports. The reason for this is unclear.

The quaternary catalysts show a trend for strong acidity which is different from that of the binary catalysts. The trend of strong acidity decreases in the order of Highest Magnesia > highest alumina > highest zirconia content in the catalyst. This trend is very different from that of the supports which is highest alumina > highest zirconia > highest magnesia content of catalyst. Thus, NiO appears to contribute significantly to the strong acidity of the catalysts in quaternary catalysts.

Compared to the acidity of the supports, ternary catalysts 7.5%Ni-AMZ-29-0-59, 7.5%Ni-AMZ-39-0-49 and quaternary catalysts 7.5%Ni-AMZ-44-22-22 and 7.5%Ni-22-22-44 show a significant decrease in strong acidity compared to the supports used for preparing them. Of these both ternary catalysts are combinations of alumina-zirconia whereas the quaternary catalysts are either rich in alumina or zirconia. Thus, there is a common thread. It is noted from the trend of acidity of the supports that ternary supports of alumina-zirconia show a significant increase in strong acidity compared to the binary alumina or zirconia supports. This increase is attributed to the formation of solid solutions, which is also indicated by the results of XRD studies (Appendix 8). Thus, the increase in acidity due to the formation of alumina-zirconia solid solutions is negated by the presence of Nickel, reason for which is not clear.

In contrast, binary catalyst 7.5%Ni-AMZ-0-89-0, ternary catalysts 10%Ni-AMZ-44-0-44, 5%Ni-AMZ-44-44-0, 5%Ni-AMZ-44-0-44 and 7.5%Ni-0-44-44 and quaternary catalyst 7.5%Ni-AMZ-22-44-22 show an increase in strong acidity relative to the support used for their preparation. All these catalysts are either magnesia based or rich in magnesia content or combinations of equal content (by weight %) of alumina with magnesia or zirconia (balanced supports)

The trend of total acidity of the catalysts is shown in Figure 28 below. Catalysts with different Ni content on support AMZ-44-0-44 are colored yellow and those with Ni supported on support AMZ-44-44-0 are colored green.

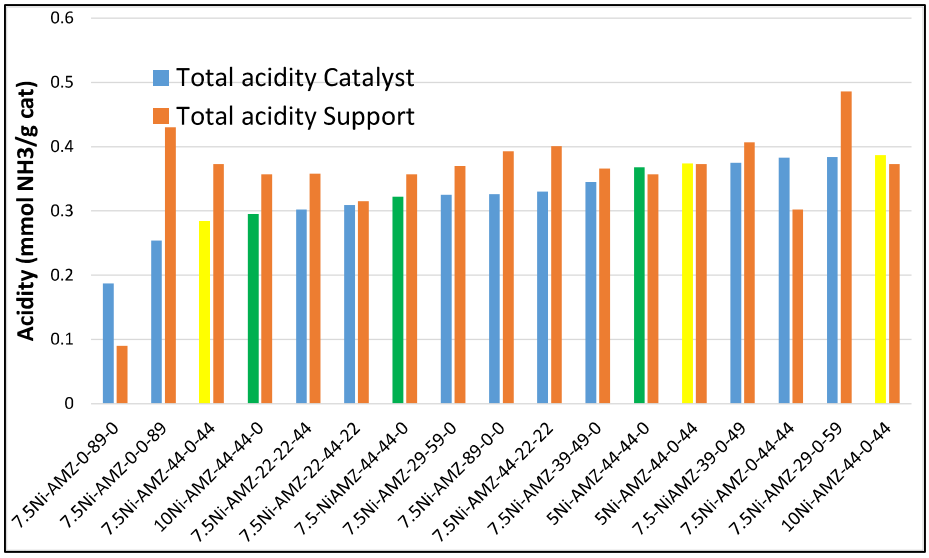

Figure 28: Trend of total acidity of supported Nickel catalysts and their corresponding supports

As seen from Figure 28, the trend of total acidity for the binary catalysts decreases in the order Al>Zr>Mg, which is similar to the trend of strong acidity. It is demonstrated in chapter 2 from the decomposition of MBOH that the binary MgO support has basic character. Wurzler et.al. [12] have shown presence of basic sites on Ni supported on MgO using CO_2 TPD. Fabien Aupretre et.al. [13] have studied $Mg_xNi_{1-x}Al_2O_3$ spinel oxides for ESR. They report that these spinels have a lower acidity which results in high stability and activity for ethanol steam reforming.

Amongst the ternary catalysts with 7.5wt% Ni, the Al-Mg catalysts do not show an increase in total acidity when Magnesia content is increased from 44% to 59%, however acidity increases when it is decreased from 59% to 49%. The ternary Al-Zr catalysts show a clear increase in total acidity with increasing zirconia content. The ternary Al-Mg catalysts show a slight decrease in acidity compared to the binary Al catalyst, whereas the ternary Al-Zr catalysts show a significant increase in total acidity. The former is consistent with that reported by Sanchez-Sanchez et.al. [10], whereas the latter is contrary. These authors have prepared the catalysts by impregnation of nitrate salts of the transition metals (other than Ni) onto an alumina support, whereas the catalysts of the current study are prepared by co-precipitation of the individual nitrates.

As regards ternary catalyst series AMZ-44-44-0 the trend of total acidity with Ni content is 5%Ni >7.5%Ni >10%Ni. Thus, increasing surface coverage of Ni decreases total acidity. The second series AMZ-44-0-44 shows 10%Ni>5%Ni>7.5%Ni (no clear trend).

Amongst the quaternary catalysts, the trend is 7.5%Ni-AMZ-44-22-22 > 7.5%Ni-AMZ-22-44-22 > 7.5%Ni-AMZ-22-22-44. Thus, a catalyst with the highest alumina content shows the highest total acidity followed by a catalyst with the highest magnesia content followed by catalyst with highest Zirconia content. (Al>Mg>Zr). This is different from that of the binary catalyst for Zr and Mg based catalysts.

Catalysts 7.5%Ni AMZ-0-89-0, 5wt% Ni-AMZ-44-44-0, 7.5%Ni-AMZ-0-44-44 and, 10wt% Ni-AMZ-44-0-44 show total acidity higher than that of their corresponding support. All the remaining catalysts show lower total acidity than their corresponding supports. A common factor between these catalysts is the presence of Magnesia in the first three catalysts.

Acid strength expressed as the peak temperature of desorption of the strong acidity peak is shown in Figure 29 below. All the samples present two peaks. The one at a lower temperature represents weak acidity whereas the one at a higher temperature represents strong acidity. Only the peak corresponding to strong acidity is shown in the Figure 29.

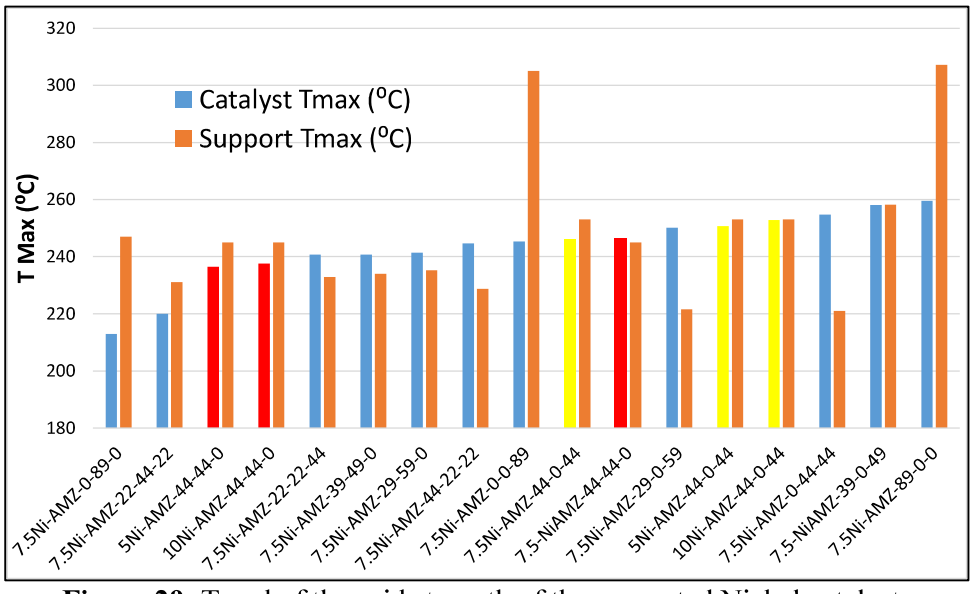

Figure 29: Trend of the acid strength of the supported Nickel catalysts

As seen from trends in Figure 29, the trend for acid strength of binary catalysts is Al>Zr>Mg. The trend is similar to the trend of strong acidity which is shown in Figure 27. There is a striking decrease in the acid strength of all three binary catalysts compared to their supports.

The ternary catalysts present the trend 7.5%Ni-AMZ-39-0-49>7.5%Ni-AMZ-0-44-44>7.5%Ni-AMZ-29-0-59>7.5%Ni-AMZ-44-44-0>7.5%Ni-AMZ-44-0-44>7.5%Ni-AMZ-29-59-0>7.5%Ni-AMZ-39-49-0. The trend is in line with the acid strength presented by the binary catalysts. The trend shows that skewed composition ternary Alumina-Zirconia (with higher zirconia) shows highest acid strength, followed by magnesia-zirconia and then alumina-magnesia. The ternary catalysts of Al-Mg and Al-Zr with balanced composition (same wt% of the two components) show stronger acid strength than ternary catalysts of Al-Mg with composition skewed of favor of Mg.

The AMZ-44-0-44 catalyst series shows a trend 10%Ni > 5% Ni > 7.5% Ni whereas the AMZ-44-44-0 catalyst series show a trend 7.5%Ni > 10% Ni >5% Ni. Thus, there is no specific trend of acid strength with Nickel content for both the series.

The quaternary catalysts show the trend: catalyst with highest Alumina content > highest zirconia > highest magnesia. This trend is similar to that of binary composites.

Catalysts 7.5%Ni-AMZ-0-44-44; 7.5%Ni-AMZ-29-0-59; 7.5%Ni-AMZ-44-22-22; 7.5%Ni-AMZ-29-59-0; 7.5%Ni-AMZ-39-49-0; 7.5%Ni-AMZ-22-22-44 show a significant increase in acid strength relative to the supports used for their preparation. Excepting for catalyst 7.5%Ni-AMZ-44-22-22, all the others are either rich in magnesia or zirconia (skewed composition). As mentioned below the balanced catalysts 7.5%Ni-AMZ-44-44-0 or 7.5%Ni-AMZ-44-0-44 either show acid strength close to that of the support or a decrease relative to the support used for their preparation.

Catalysts 7.5%Ni-AMZ-44-44-0; 5%Ni-AMZ-44-0-44, 10%Ni-AMZ-44-0-44, and 7.5%Ni-AMZ-39-0-49 show acid strength close to that of the support used for their preparation. Excepting for the first catalyst all the remaining are ternary Al-Zr catalysts.

Catalysts 7.5%Ni-AMZ 89-0-0, 7.5%Ni-AMZ-0-89-0, 7.5%Ni-AMZ-0-0-89, 5%Ni-AMZ-44-44-0, 10%Ni-AMZ-44-44-0, 7.5%Ni-AMZ-44-0-44, 7.5%Ni-AMZ-22-44-22 show acid strength less than that of the support used for their preparation. All three binary catalysts show the highest decrease in acid strength relative to the supports

used to prepare them. Amongst ternary catalysts of alumina and magnesia or alumina and zirconia those with balanced composition show this trend.

Amongst quaternary catalysts only the catalyst with the highest magnesia content shows a decrease in acid strength relative to the supports used for their preparation. The remaining two AMZ-44-22-22 and AMZ-22-22-44 show an increase in acid strength relative to their supports.

3.5: Reducibility of NiO in the catalysts: Temperature Programmed Reduction (TPR)

The reducibility of nickel oxide to Ni metal in the calcined supported catalysts was studied by TPR (Temperature Programmed Reduction). A Micromeritics Autochem-2920 instrument was used for this purpose. Samples are first heated in air to 500°C in Helium gas at 50 ml/min to remove adsorbed substances. They are then cooled to 50°C in Helium flow at 50 ml/min. A calibration gas mixture with a composition of 10 vol% Hydrogen balance Nitrogen is used for reduction. The TPR is recorded by ramping the temperature from 50°C to 900°C at 10°C/min in a flow of 10 vol% Hydrogen balance Nitrogen Gas. A cold trap is used for trapping moisture formed during reduction. The consumption of H_2 as a function of temperature is determined from the data. The stoichiometry for chemical reduction with H_2 is 1:1 for NiO:H_2 molar ratio.

Profiles of H_2 consumption as a function of temperature are shown in Figures 7.1 to 7.17 in Appendix 7. It is seen from these Figures that all the catalysts show a fairly low-temperature peak in the temperature range of 250°C-380°C. This temperature is too low for the reduction of NiO and it is present in all the catalysts irrespective of the composition of the support. Hence, it is attributed to the reduction of CeO_2 which is present in all the catalysts to an extent of nominal 5.4 wt%. Complete reduction of CeO_2 requires only 0.144 mmol H_2/g catalyst, which is significantly smaller than the lowest value of H_2 consumption 0.401 mmol H_2/g catalyst for binary Mg catalyst 7.5%Ni-AMZ-0-89-0.

While some catalysts show a single peak, some show two peaks. The terms "lower" and "higher" temperature is used to differentiate between peaks with maxima lower than 500°C and higher than 500°C respectively. This holds for most of the

catalysts. Only two catalysts do not conform to this classification. Binary AMZ-0-89-0 presents a low-temperature peak at 284.6°C and a high-temperature peak at 463.8°C. Whereas catalyst AMZ-89-0-0 presents a low-temperature peak at 627.8°C and a high-temperature peak at 722.3°C.

The trend of peak temperature of reduction (Tmax of TPR peaks) is shown in Figure 30 below.

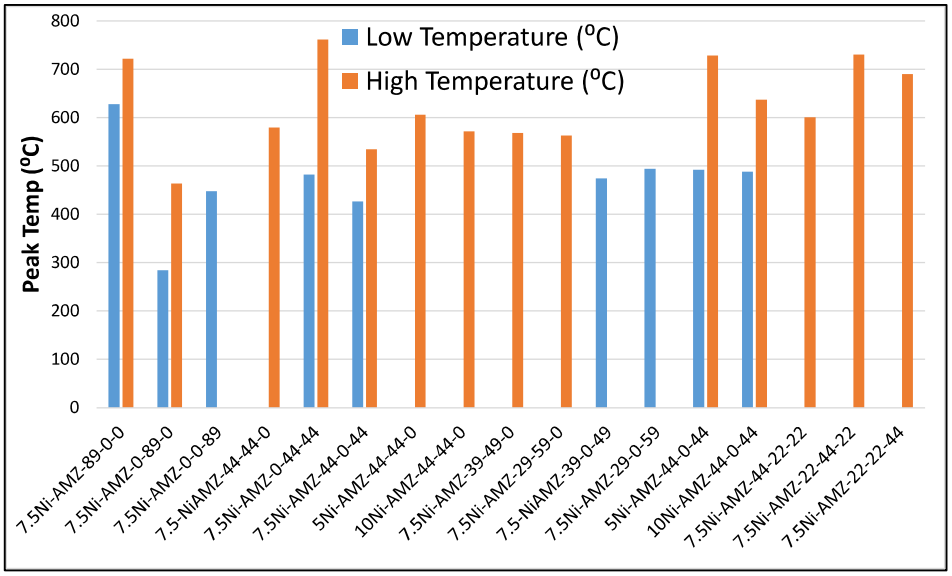

Figure 30: Peak maxima of low and high-temperature peaks in TPR of supported Nickel metal catalysts.

The following inferences are drawn from Figure 30:

Inferences for Binary catalysts

- Amongst the binary catalysts, the trend of the low-temperature peak is Alumina (628°C) > Zirconia (448°C) > Magnesia (285°C) based catalysts, indicating that interaction of Ni with the support decreases in that order. The trend of the high-temperature peak is Alumina (722°C) > Magnesia (464°C). Zirconia presents a single peak, which by the definition used in this study is classified as the low-temperature peak. Becerra et.al. [14] have reported TPR of pure NiO, $NiAl_2O_4$ and NiO impregnated as its nitrate on γ-Al2O3 followed by calcination at 900°C. According to their studies NiO reduces at 390°C, whereas $NiAl_2O_4$ reduces at 917°C and the NiO in the supported metal catalyst calcined at 900°C reduces at 850°C. Thus, nickel aluminate reduces at a significantly high

temperature. Cerritos et.al. [15] have studied 5-10%Ni impregnated on Al_2O_3-La_2O_3 prepared by the sol gel method. They report a broad reduction peak 77°C -577°C and another high temperature peak at about 777°C temperature. They attribute these to NiO with weak and strong interaction with the support respectively. The reduction temperature of NiO in the binary Al catalyst of the current study is in between that reported by both Becerra et.al. and Cerritos et.al. Seung Ju Han et.al. [8] have studied the effect of Zr/Al in Ni-Al_2O_3-ZrO_2 xerogel catalysts for ESR. Their catalysts are prepared by single step sol gel method using epoxide. They report reduction maxima 638°C for Ni/Al_2O_3 and appearance of a low temperature peak in the range 454-486°C in catalysts promoted with zirconia. They attribute the high temperature peak to NiO interacting with alumina and the low temperature peak to NiO interacting with ZrO_2. Both these values are close to those obtained in the current study. Shuirong Li et.al [7] have reported reduction of NiO at 306°C for conventional catalysts prepared by precipitation and impregnation whereas 450°C (higher temperature) for catalysts prepared by gelation of ZrO_2 in presence of NiO nanoparticles. They infer that the latter results in stronger metal oxide-support interaction which lends stability to the catalyst in ESR. In the current study only a low temperature reduction peak at 448°C was observed for Ni supported on binary zirconia (AMZ-0-0-89). The value of this peak is close to that reported by Li et.al. for NiO@ZrO_2 nanocomposite catalyst. As seen from subsequent chapters, catalysts containing zirconia do show better stability. Benito et.al. [18] have studied 10% Ni impregnated on ZrO_2 prepared by calcination of its hydroxide at 800°C. The impregnated catalysts are calcined at 750°C. They report reduction of NiO at 643°C and 823°C. The higher reduction temperature appears to be due to the higher calcination temperature used in their study

- Further, the maxima of the magnesia-based catalyst (7.5%Ni-AMZ-0-89-0) is significantly low (284.6°C) whereas the value for the next highest low-temperature peak is 426.6°C (7.5%Ni-AMZ-44-0-44). Its high-temperature peak is at 463.8°C. Thus, the magnesia-based binary catalyst shows the weakest metal-support interaction with Nickel not only within the binary catalyst series but across all catalysts studied in this work. However, based on values of extent of reduction of Ni oxide (Figure 31 below) it is observed that only a portion of

the oxide reduces at these temperatures in this catalyst, indicating that there is a fraction of Ni oxide which interacts strongly with Mg and does not reduce even at 800°C. This is attributed to formation of NiO-MgO solid solution which is supported by results of XRD. Wurzler et.al. [12] have reported similar behaviour. Frusteri et.al [5] have also reported two peaks one each at 280°C and 700°C for Ni supported on MgO. They attribute the high temperature peak to NiO which is located in the lattice of MgO. The first peak reported by Frusteri et.al. [5] is comparable to that obtained in the current study (284°C) for AMZ-0-89-0, whereas the latter is at significantly higher temperature 700°C against 464°C observed in the current study. Wurzler et.al. [12] have reported reduction of NiO which is supported on MgO at temperatures ranging from 555-587°C (low temperature peak) and 710°C-1055°C (high temperature). Since the degree of reducibility of NiO was low (32%) in the current work when the catalyst is reduced at 800°C for TPR), it is evident that some of the NiO which reduces at high temperature remained unreduced.

- Zirconia-based catalyst 7.5%Ni-AMZ-0-0-89 shows only one (low) temperature peak (447.8°C) indicating weak metal (Nickel)-support interaction. Since this catalyst shows complete reduction of NiO (Figure 31 below), the interaction is deemed to be truly weak.

Inferences for Ternary catalysts

- All the catalysts based on alumina-magnesia combination show only a high temperature peak in the range 563°C - 579°C for equitable Ni content. This temperature decreases with increasing Mg content of the catalyst. The catalysts with balanced composition of Al and Mg 44-44-0 series show a decreasing trend with Ni content: 606°C (5wt% Ni), 579.5°C (7.5wt%Ni) and 572°C (10wt% Ni). These catalysts present a single high temperature peak irrespective of whether the alumina and magnesia content is balanced or skewed towards magnesia. The maxima of this peak ranges from 564°C - 606°C across this series of catalysts. For Ni content at 7.5 wt% the peak temperature of reduction decreases with increasing magnesia content of the ternary Al-Mg catalysts indicating a slight decrease in interaction of NiO with the support.

- Further, the value of peak maxima of this series of support decreases with increasing Ni content in this series. The trend is 5%Ni-AMZ-44-44-0 (606°C) > 7.5%Ni-AMZ-44-44-0 (579°C) > 10%Ni-AMZ-44-44-0 (572°C). Thus, as NiO content exceeds the concentration required for the formation of a monolayer, its interaction with the support decreases.
- The ternary alumina-zirconia catalysts show a different behaviour. Only catalysts with balanced content of alumina-zirconia (AMZ-44-0-44 series) show two peaks. A low temperature peak in the region 426°C-492°C and a high temperature peak in the region 534°C-728°C.
- The trend of the low-temperature peak of this ternary Al-Zr series of support with Ni content is 5%Ni-AMZ-44-0-44 (492°C) > 10%Ni-AMZ-44-0-44 (488°C) > 7.5%Ni-AMZ-44-0-44 (427°C) while the trend of the high-temperature peak is 5%Ni-AMZ-44-0-44 (728°C) > 10%Ni-AMZ-44-0-44 (637°C) > 7.5%Ni-AMZ-44-0-44 (535°C). Thus, there is no clear trend with Ni content.
- Ternary catalysts of alumina-zirconia with composition skewed in favour of zirconia (7.5%Ni-AMZ-29-0-59 (494°C) and 7.5%Ni-AMZ-39-0-49 (474°C) show only single peak (value shown in braces), similar to the binary zirconia catalyst (Tmax 448°C). Thus, Tmax increases with increase in zirconia content. Seung Ju Han et.al. [8] who have studied the effect of Zr/Al in Ni-Al_2O_3-ZrO_2 xerogel catalysts for ESR also report an increase in the maxima of this peak from 486°C to 545°C upon increasing ZrO_2 content from 20% to 40%. The behaviour of ternary Al-Zr catalysts is in contrast to that of ternary Al-Mg catalysts where Tmax decreases with increasing magnesia content. Binary alumina catalyst shows two peaks at 628°C and 722°C, which is not reflected in its ternary composition with Zr. Since Al has a smaller ionic radius than Zr it is expected that the Al in composites with lower Al content is more likely to exist in the form of solid solution in zirconia. Thus, this appears to be the reason that these composites behave similar to zirconia (weak interaction with NiO). Whereas, catalysts with balanced alumina-zirconia (AMZ-44-0-44 series) appear to have at least some alumina which is segregated from zirconia (not existing as solid solution) hence presenting two peaks. Overall, the ternary Al-Zr catalysts show lower peak temperature of reduction than the ternary Al-Mg

catalysts. Also, the binary Zr catalyst shows a low temperature peak at 447.8°C which falls within the temperature range of low temperature peak of all the ternary Al-Zr catalysts (426-494°C) indicating that an excess zirconia phase could be present which interacts differently with NiO. This is supported by results of XRD which do show presence of t-ZrO_2 in this catalyst.

- All three quaternary catalysts show a single high temperature peak in the range 601°C to 731°C. Trend in decreasing order of temperature is 7.5%Ni-AMZ-22-44-22 > 7.5%Ni-AMZ-22-22-44 > 7.5%Ni-AMZ-44-22-22. Thus, the catalyst with highest magnesia shows the highest temperature followed by the one with highest zirconia and then highest alumina. This trend is the exact opposite of the trend of binary catalysts which is alumina > magnesia and zirconia not presenting a high temperature peak. Binary zirconia presents only one peak at 447.8°C. These striking changes from binary to quaternary compositions are attributed to formation of solid solution in case of zirconia-alumina and magnesium aluminate spinel in case of magnesia-alumina. XRD results support this contention. Thus, the interactions between components of the support in ternary and quaternary catalysts results in a change in their interaction with NiO (relative of binary catalysts).
- The catalyst comprising balanced contents of magnesia and zirconia as key components of the support shows two peaks. A low-temperature peak at 482°C and a high-temperature peak at 762°C. The value of the high-temperature peak is the highest among all the catalysts studied, indicating the strongest interaction of Nickel with this support.
- Amongst the ternary and quaternary catalysts, those rich in zirconia and/or magnesia show a significantly higher value of the high-temperature peak. 7.5%-AMZ-0-44-44 (762°C) > 7.5%Ni-AMZ-22-44-22 (731°C) ≥ 5%Ni-AMZ-44-0-44 (728°C) > 7.5%-AMZ- 22-22-44 (690°C)

The trends of Hydrogen consumption at low temperature, high temperature and total consumption are shown in Figure 31:

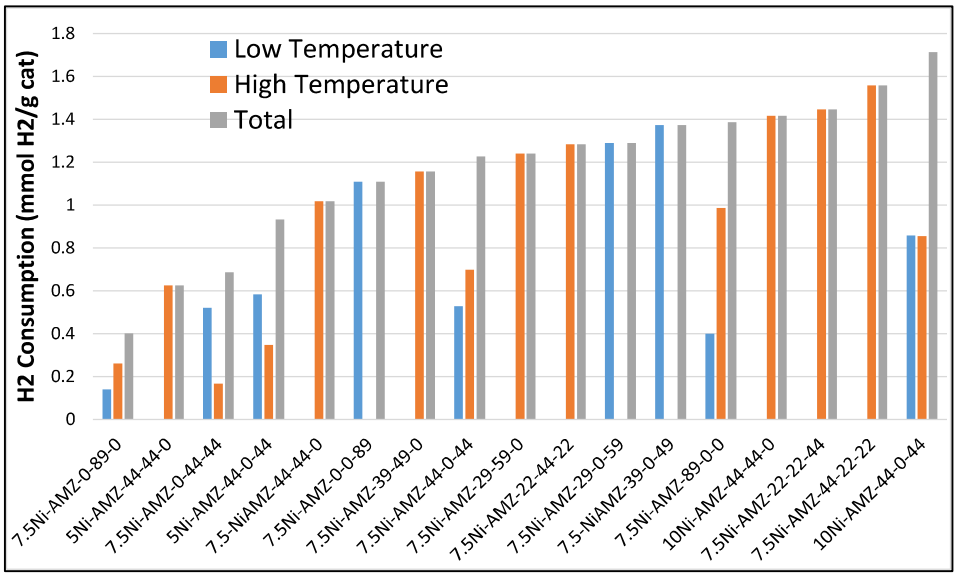

Figure 31: Total H_2 consumption with the breakup of consumption at low and high temperatures

As seen from Figure 31, the binary catalysts show the following trends. H_2 consumption at low temperature (<500°C) decreases in the order Zr>Al>Mg. The trend of H_2 consumption at high temperatures is Al>Mg. Zirconia does not show a high-temperature peak. However, the temperature of the low-temperature peak of zirconia (448°C) is close to that of the high-temperature peak of magnesia (464°C).

The ternary catalysts show the trend 7.5%Ni-AMZ-39-0-49 > 7.5%Ni-AMZ-29-0-59>10%Ni-AMZ-44-0-44>5%Ni-AMZ-44-0-44>7.5%Ni-AMZ-44-0-44=7.5%Ni-AMZ-0-44-44 for the low temperature peak. At constant Nickel content (7.5wt%) alumina-zirconia catalysts with a composition skewed in favor of zirconia show higher H_2 consumption at the lower temperature than catalysts with a balanced composition of alumina and zirconia. Alumina-magnesia ternary catalysts do not present low-temperature peaks. Ternary catalysts of magnesia-zirconia show the lowest H_2 consumption within the ternary catalysts. The value is close to that of a balanced alumina-magnesia catalyst.

The quaternary catalysts do not present a peak at low temperatures.

As regards H_2 consumption at high temperatures (>500°C), it decreases in the order Al>Mg for the binary catalysts. The zirconia-based catalyst shows a peak at 448°C which is classified as a low temperature peak in this work. The ternary catalysts show a decreasing trend in H_2 consumption at a high temperature which is 10%Ni-

AMZ-44-44-0>7.5%Ni-AMZ-29-59-0>7.5%Ni-AMZ-39-49-0>7.5%Ni-AMZ-44-44-0>10%Ni-AMZ-44-0-44>7.5%Ni-AMZ-44-0-44>5%Ni-AMZ-44-44-0>5%Ni-AMZ-44-0-44>7.5%Ni-AMZ-0-44-44. For constant Nickel content at 7.5 wt% the trend indicates that alumina-magnesia composites whose composition is skewed in favor of magnesia show higher H_2 consumption at high temperature than catalysts with balanced alumina-magnesia composition. Alumina-zirconia-based ternary catalysts with composition skewed in favor of zirconia do not present high-temperature peaks. While the one with balanced alumina and zirconia present a high-temperature peak whose H_2 consumption is lower than that of corresponding alumina-magnesia catalysts. Thus alumina-zirconia facilitates the reduction of Nickel at a lower temperature than alumina-magnesia-based catalysts.

Both the AMZ-44-0-44 and AMZ-44-44-0 series shows an increasing trend of H_2 consumption with increasing Nickel content, which is consistent with theoretical expectation.

The quaternary catalysts show only a high-temperature peak. The trend of decreasing H_2 consumption is the catalyst with the highest alumina content > highest zirconia content > highest magnesia content.

The trend of total H_2 consumption in decreasing order for binary catalysts is Al>Zr>Mg.

The trend of ternary catalysts is 10%Ni-AMZ-44-0-44>10%Ni-AMZ-44-44-0>7.5%Ni-AMZ-39-0-49>7.5%Ni-AMZ-29-0-59>7.5%Ni-AMZ-29-59-0>7.5%Ni-44-0-44>7.5%Ni-39-49-0>7.5%Ni-44-44-0>5%Ni-AMZ-44-0-44>7.5%Ni-AMZ-0-44-44>5%Ni-AMZ-44-44-0. This trend shows the expected trend of decrease in total H_2 consumption with a decrease in Nickel content for both the AMZ-44-0-44 and AMZ-44-44-0 series. Further, for constant Nickel content at 7.5wt%, the trend shows that alumina-zirconia-based catalysts show higher total H_2 consumption than alumina-magnesia catalysts. The magnesia-zirconia-based catalyst shows the lowest total H_2 consumption. Thus, NiO supported on alumina-zirconia supports is more easily reduced than NiO supported on alumina-magnesia based supports at the conditions used in the current TPR studies.

The fractional reducibility of NiO based on moles of H_2 consumed per mole NiO during TPR is shown in Figure 32 below. The theoretical value for this is 1.0. This is marked by a horizontal line in Figure 32

$$NiO + H_2 = Ni(0) + H_2O$$

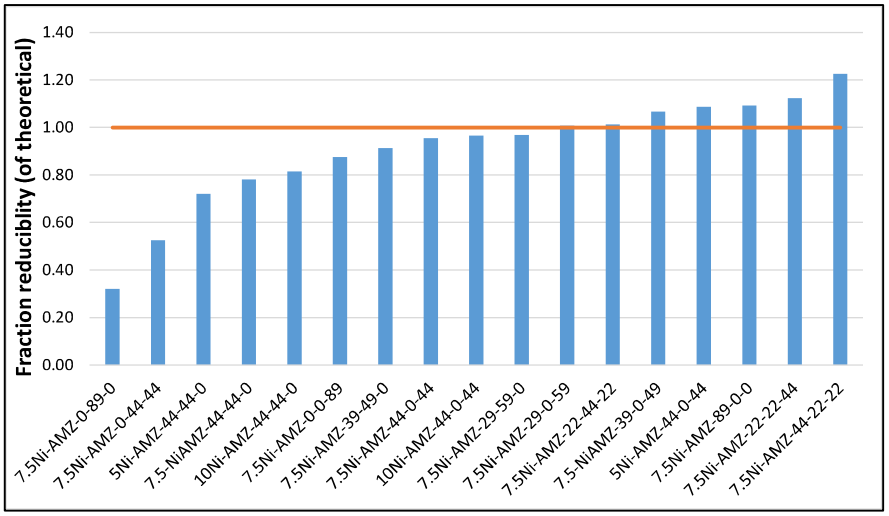

Figure 32: Fractional reducibility of NiO of the supported metal catalysts

The experimental values are calculated from the moles of H_2 consumed and the mole of NiO determined by ICP-OES analysis.

As seen from Figure 32, the fractional reducibility trend of Ni supported on the binary catalysts under the conditions of reduction of the TPR experiment is Al (1.09) > Zr (0.88) >>Mg (0.32). Thus, both zirconia and magnesia (to a much larger extent) inhibit the reduction of NiO. Although Tmax is significantly higher for alumina catalysts compared to magnesia and zirconia catalysts, the results of TPR indicate that some portion of Ni remains in oxide form in the latter two catalysts despite reduction at 800°C. Biswas et.al. [6] have studied 10-40 wt% Nickel supported CeO_2, ZrO_2 and mixed oxides of ceria and zirconia with CeO_2/ZrO_2 weight ratio varying from 0.25-4. The supports are prepared by co-precipitation and Nickel is impregnated by incipient wetness. They report a 97.3% reduction of the 10 wt% Nickel catalyst supported on $Ce_{0.74}Zr_{0.26}O_2$ support. The reducibility of NiO in the binary 0-0-89 catalyst in the present study is slightly lower (about 87.6%). A reason for this could be the lower Ni content used in the current study. Tatiana de Freitas Silva et.al. [19] have studied 15% Ni/Al_2O_3 promoted by impregnation with Ce, La and Zr. They report degree of

reduction 86% for NiO/γ-Al_2O_3 catalyst and 100% for NiO/CeO_2-ZrO_2-Al_2O_3. These results are contrary to those observed in the current study.

Frusteri et.al [5] have studied 21 wt% Nickel impregnated of MgO. They report a dispersion of 14% upon reduction of Nickel at 750°C due to the formation of a solid solution of Nickel with MgO. The degree of reducibility reported is around 80-82%. In the present study Nickel content is significantly lower (7.5wt%) which increases metal-support interaction because of which degree of reducibility of Nickel is observed to be just 32% even at 800°C. Wurzler et.al. [12] have studied 5wt% Nickel supported on MgO supports prepared by precipitation to a final pH 10 with ageing (12 hours) and without ageing and also MgO prepared by thermal decomposition of the nitrate at 500°C for 2 hours. The Nickel is impregnated on the latter support and the catalyst calcined at 400°C (3 hours). They report the degree of reducibility of Nickel at 74%, 31% and 42% respectively for these three catalysts. The values for the latter two catalysts are comparable with the values obtained in the current study (32%). The value for the catalysts prepared by precipitation of MgO without aging match closely with the value of 0-89-0 obtained in the current study. Wurzler et.al. [12] estimate from in-situ XANES that 39%, 63% and 50% of Nickel exists as a solid solution in these catalysts respectively. They attribute XRD peaks at 2θ 37.2° 2θ and 43.1° 2θ to NiO-MgO solid solution. As seen from Figure 33 (a) below the XRD for catalyst 7.5%Ni-AMZ-0-89-0 does show peaks at these 2θ. The intensity of the former peak is larger than that of the latter in this catalyst. Thus, it differs from the XRD pattern of NiO which also has peaks at these two 2θ values but with the latter peak having stronger relative intensity (100%) whereas the peak at 37.2° 2θ has intensity 61%. The other two binary catalysts 7.5%Ni-AMZ-89-0-0 (Figure 33(b)) and 7.5%Ni-AMZ-0-0-89 (Figure 33(c)) show XRD peaks which can be attributed to NiO. MgO (Periclase) also has a peak at 36.93° 2θ, however its relative intensity is very low 4% in 7.5%Ni-AMZ-0-89-0. Wurzler et.al. [12] also report through in-situ XRD studies that reduction at 1023°K destroys the solid solution releasing Ni as metallic particles. In the current work the binary 7.5%Ni-0-89-0 (Mg based catalyst, Figure 33(a)) shows very broad weak diffused peaks of NiO, whereas 7.5% Ni-89-0-0 (alumina-based catalyst) and 7.5%Ni-0-0-89 (Zr based catalyst), Figures 33(b) and 33(c) respectively) show sharp intense peaks at 43.27° 2θ.

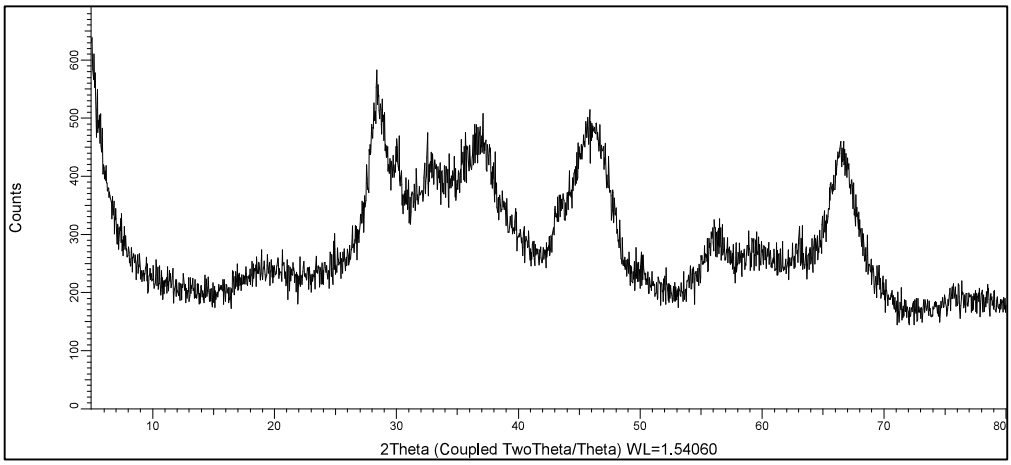

Figure 33 (a): XRD pattern of 7.5%Ni-0-89-0

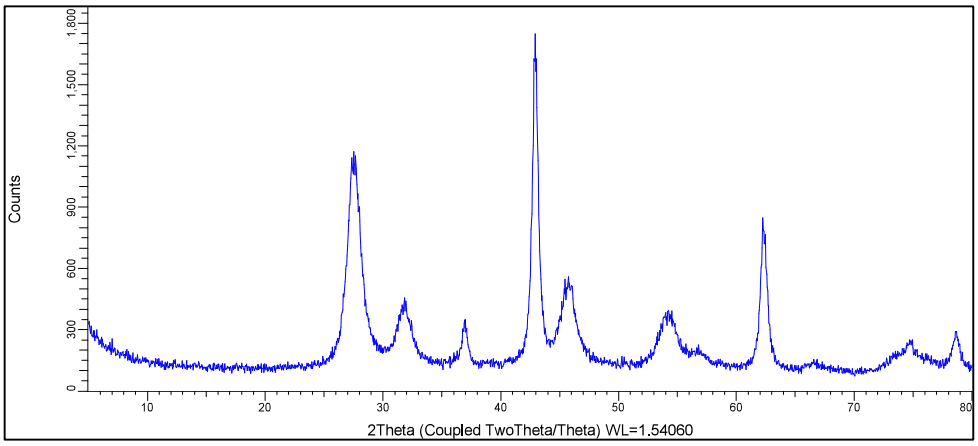

Figure 33 (b): XRD pattern of 7.5%Ni-89-0-0

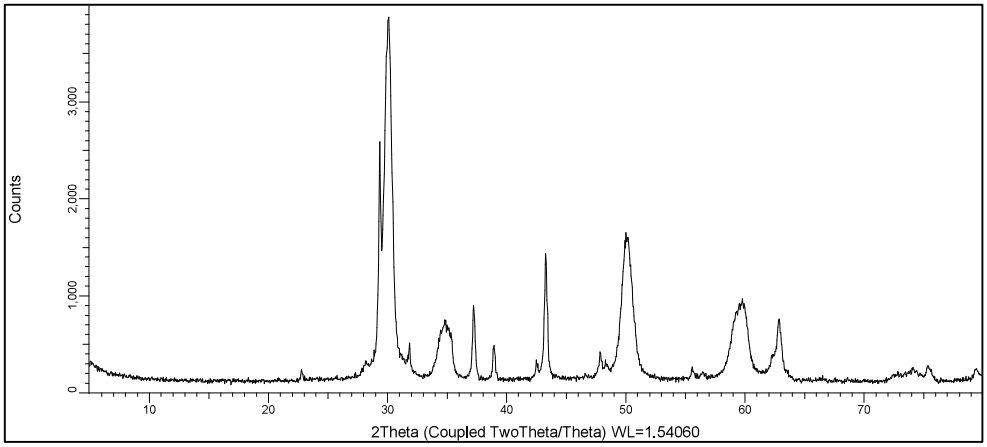

Figure 33 (c): XRD pattern of 7.5%Ni-0-0-89

This indicates that the NiO exists as a solid solution in the binary MgO support.

This trend also reflects in the lower values of dispersion of these two catalysts relative to the alumina-based catalyst due to the low reducibility of NiO (Figure 32).

As regards ternary catalysts, all three catalysts of AMZ-44-44-0 (balanced alumina – magnesia series) with Nickel content varying from 5 to 10wt% show reducibility less than the theoretical maximum (0.52 to 0.82). Within these, the catalysts with 5% and 7.5% Nickel content show lower reducibility of NiO than the catalyst with 10wt% Nickel. The trend of fractional reducibility of NiO is 10%Ni-AMZ-44-44-0 (0.82) > 7.5%Ni-AMZ-44-44-0 (0.78) >5%Ni-AMZ-44-44-0 (0.72). The trend is consistent with lower metal-support interaction (and hence higher reducibility) with increasing concentration of Nickel. It is also noted that the values are short of the theoretical maximum which is consistent with the trend of binary catalyst 7.5%Ni-AMZ-0-89-0, which shows that a good part of NiO remains unreduced in the magnesia-based catalysts.

The catalysts with composition skewed in favor of magnesia show higher values of fractional reducibility, with the value approaching the theoretical maximum with increasing magnesia content. The trend is 7.5%-AMZ-29-59-0 (0.97) > 7.5%-AMZ-39-49-0 (0.91). This is contrary to the trend of binary catalysts wherein magnesia-based catalyst shows significantly poor reducibility. Thus, the inclusion of a smaller quantity of alumina in magnesia appears to improve the reducibility of NiO on the support. XRD indicates formation of $MgAl_2O_4$ spinel which could be responsible for the difference.

All ternary catalysts based on alumina-zirconia combination show reducibility close to the theoretical maximum. Values range from 0.954 (for 7.5%Ni-AMZ-44-0-44) to 1.087 (5%Ni-AMZ-44-0-44). There is no difference between catalysts with balanced and skewed alumina zirconia content. Thus, NiO reduces almost completely in these catalysts.

All three quaternary catalysts show fractional reducibility of NiO equal to or exceeding the theoretical maximum by 7%-22%. Of these 7.5%Ni-AMZ-22-22-44 (1.123) and 7.5%Ni-AMZ-44-22-22 (1.226) show reducibility exceeding the theoretical maximum. Binary 7.5%Ni-AMZ-89-0-0 (1.093) and ternary 7.5%Ni-AMZ-39-0-49 (1.067) also show reducibility exceeding the theoretical maximum. H_2 consumption exceeding the theoretical maximum is indicative of spillover of H_2 to the support. However, since the supports contain about 4.95 wt% ceria, it is also possible that the excess H_2 consumption over the theoretical value for reduction of Ni is due to contribution from the reduction of ceria. The theoretical quantity of H_2 required for the

complete reduction of ceria is less than 10% of that required for the reduction of NiO in the supported metal catalysts.

3.6: Dispersion of Nickel

Dispersion of active metal (Nickel in this particular case) is important for the activity of supported metal catalysts. Dispersion of Nickel was determined by first reducing a known weight of the dry catalyst in flowing H_2 at 550°C. The H_2 was desorbed at 120°C in flowing N_2 and the catalyst was cooled to room temperature in N_2. Metal dispersion was determined by pulsing O_2 and determining the total quantity of O_2 consumed per gram catalyst or g Nickel metal in the catalyst. Molar stoichiometry 1 Ni = $1O_2$ was used for determining dispersion. Nickel metal surface area was calculated using the total volume of O_2 consumed.

The trend of dispersion expressed as the specific surface area of Nickel metal is shown in Figure 34 below. Catalyst series in which Ni content is varied are colored yellow (AMZ-44-0-44) and red (AMZ-44-44-0)

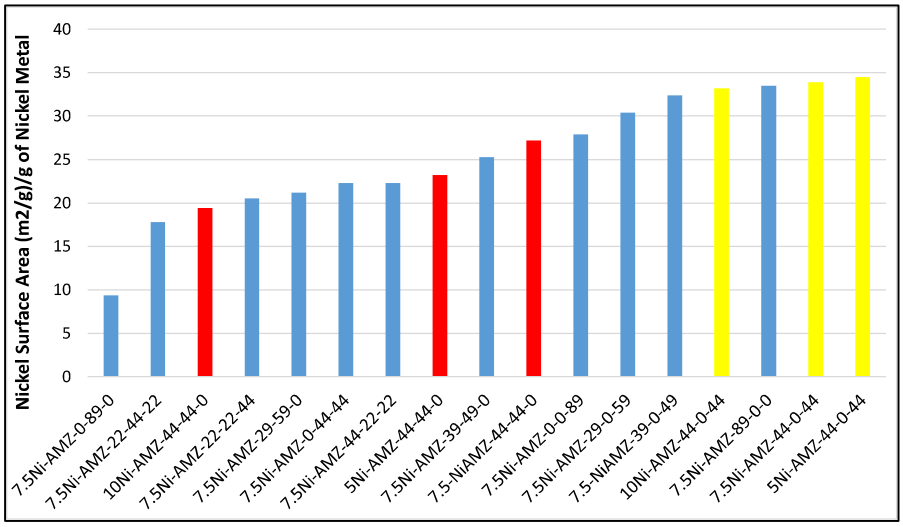

Figure 34: Specific surface area of Nickel in the supported metal catalysts

As seen from trends in Figure 34 above, amongst the binary series of catalysts specific surface area of Nickel decreases in the order Al>Zr>>Mg. Further, the values of specific surface area of Ni supported on alumina (7.5%Ni-AMZ-89-0-0) is amongst the highest within the entire series of catalysts studied, whereas the values of specific surface area of Ni supported on magnesia (7.5%Ni-AMZ-0-89-0) based binary support is amongst the lowest. The metal surface area correlates with that of the BET specific

surface area of the support used to prepare the binary catalysts. Higher the BET specific surface area of the binary catalyst support, higher the metal surface area of Ni metal. Yaakob et.al. [4] have studied 5% Ni impregnated on alumina prepared by sol-gel. They report Ni surface area 1.75 $m^2/g/g$ Ni for the catalysts whose support is calcined at 600°C and 19-21 $m^2/g/g$ Ni for catalysts which are calcined at 800°C-900°C. In the current study Ni surface area is 33.5 $m^2/g/g$ Ni which is closer to that of the catalysts calcined at higher temperature in the study carried out by Yaakob et.al. [4]. Paula Osorio-Vargas et.al. [20] have studied 10% Ni/Al_2O_3 catalysts promoted by impregnation of precursors of La_2O_3 and CeO_2 for ESR. They report Ni surface area in the range 8.15-8.72 $m^2/$ g cat which is significantly lower than that observed in the current study. A possible reason could be the higher Ni content and also the lower BET surface area of their samples which range from 94 to 189 m^2/g catalyst. Tatiana de Freitas Silva et.al. [19] have studied 15% Ni/Al_2O_3 promoted by impregnation with Ce, La and Zr. They report Ni metal surface area in the range 10.2 to 13.8 $m^2/$ g catalyst. This is also lower than that achieved in the current study probably due to the higher Ni content and lower BET surface area of the supports used in their study. Fusteri et.al. [5] have studied 21 wt% Nickel impregnated of MgO. They report a Ni-metal surface area of 6.3 m^2/g cat. The value for binary MgO catalyst (7.5%Ni-AMZ-0-89-0) in the current study is 9.4 m^2/g catalyst. The higher value is expected to be due to the lower Nickel content in the current study.

As regards the ternary series of catalysts, the trend of Nickel metal surface area for catalysts with constant 7.5wt% Nickel content is 7.5%Ni-AMZ-44-0-44>7.5%Ni-AMZ-39-0-49>7.5%Ni-AMZ-29-0-59>7.5%Ni-AMZ-44-44-0>7.5%Ni-AMZ-39-49-0>7.5%Ni-AMZ-29-59-0>7.5%Ni-AMZ-0-44-44. Based on this trend the dispersion of Ni is highest on ternary catalysts based on alumina-zirconia followed by those based on alumina-magnesia and lastly magnesia-zirconia. The incorporation of alumina with zirconia or magnesia in ternary catalysts significantly improves dispersion (relative to binary zirconia or magnesia catalysts).

The trend of BET-specific surface area of the supports of the ternary catalysts with constant Nickel content (7.5wt%) is AMZ-44-0-44>AMZ-39-0-49>AMZ-29-0-59>AMZ-44-44-0>AMZ-39-49-0>AMZ-29-59-0>AMZ-0-44-44. The trend correlates well with that of Nickel metal surface area. Thus, similar to the binary catalysts the

dispersion of Nickel in ternary catalysts is dependent on the BET-specific surface area of the support.

Within the ternary series, dispersion of Nickel shows the expected trend 5%Ni-AMZ-44-0-44 (34.5m^2/g) > 7.5%Ni-AMZ-44-0-44 (33.9 m^2/g) > 10%Ni-AMZ-44-0-44 (33.2 m^2/g) for the series of catalysts based on alumina-zirconia. Metal particle size is expected to increase with increasing metal content. The ternary catalysts based on alumina-magnesia do not show a clear trend 7.5%Ni-AMZ-44-44-0 (27.2 m^2/g) > 5%Ni-AMZ-44-44-0 (23.2 m^2/g) > 10%Ni-AMZ-44-44-0 (19.4 m^2/g). The reason for this is attributed to the differences in the extent of reduction of Ni in these catalysts (Figure 31), which is 5%Ni-AMZ-44-44-0 (0.72 mass fraction) 7.5%Ni-AMZ-44-44-0 (0.78 mass fraction) 10%Ni-AMZ-44-44-0 (0.82 mass fraction).

As regards the quaternary series of catalysts. The trend is 7.5%Ni-AMZ-44-22-22 (26.9 m^2/g) > 7.5%Ni-AMZ-22-22-44 (20.5 m^2/g) > 7.5%Ni-AMZ-22-44-22 (17.8 m^2/g). Thus, catalysts rich in alumina show the highest dispersion of Nickel followed by catalysts rich in zirconia and lastly catalysts rich in magnesia. The trend is similar to that for binary catalysts. Again, the dispersion of Nickel is dependent on the BET-specific surface area of the support.

The surface area of Nickel of the entire set of 17 catalysts is regressed with the BET-specific surface area of the catalyst (from N_2 physisorption studies) in Figure 35 below. It is observed that the correlation is poor. The correlation constant is 0.5794. Several outliers are observed which contribute to the poor correlation. These include catalysts with Nickel content other than 7.5wt%.

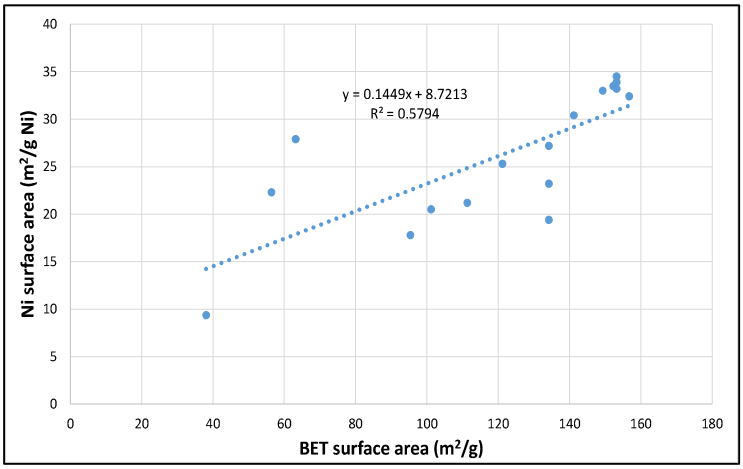

Figure 35: Trend of the specific surface area of Nickel versus BET surface area of support used for the preparation of the catalyst.

Figure 36 below correlates Nickel metal surface area as a function of BET-specific surface area of catalysts with constant Nickel content (7.5wt%).

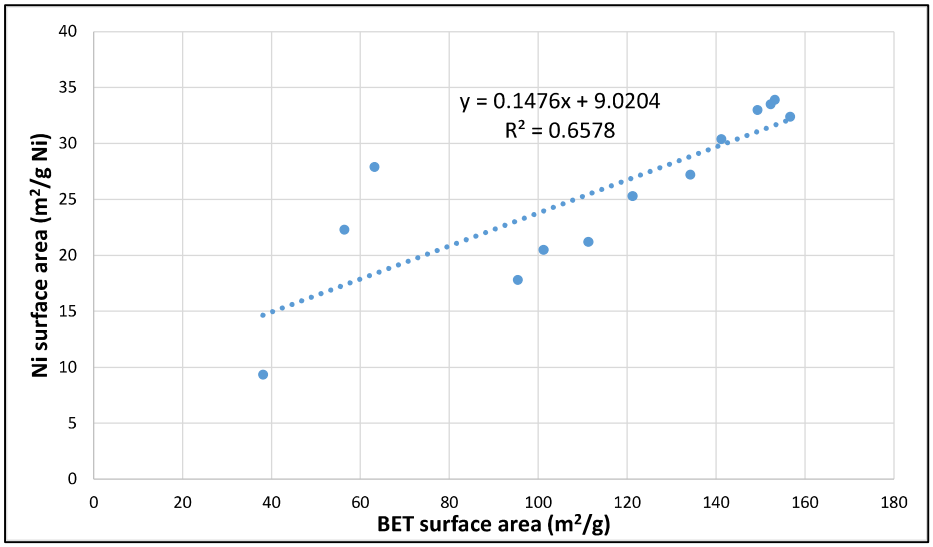

Figure 36: Trend of the specific surface area of Nickel versus BET surface area of support used for the preparation of the catalyst with constant Nickel content (7.5wt%).

There is an improvement in the correlation constant to 0.6578. Now key outliers are the catalysts that show a poor degree of reducibility in TPR studies, viz. 7.5%Ni-0-89-0, 7.5%Ni-0-0-89 and 7.5%Ni-0-44-44. A striking commonality between the outliers is low BET-specific surface area in the case of all three and the presence of magnesia in the support of two of these catalysts (which hinders the reduction of Ni).

Xiaoyong Wang et.al [16] have studied the dispersion capacities of NiO on γ-Al_2O_3. They report a monolayer capacity of 0.14g NiO/100m^2 area of support. Using this relation, the ratio of amount of NiO that can be accommodated as a monolayer on a given support to the actual NiO content per gram of that support was calculated. This value is plotted against the surface area of Ni determined by O_2 chemisorption in in Figure 37 below.

As seen from this Figure, except for AMZ-0-89-0 where this ratio is 0.78, all the remaining catalysts show a good linear relation. The actual dispersion of Ni determined by the chemisorption of O_2 correlates reasonably well with this ratio. All the catalysts considered have Ni content of 7.5wt%.

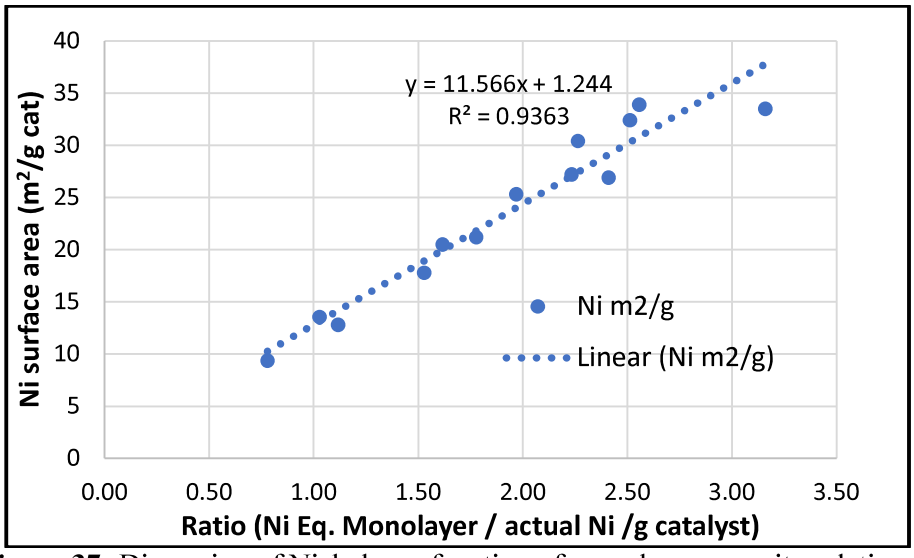

Figure 37: Dispersion of Nickel as a function of monolayer capacity relative to Nickel content per gram catalyst

Since magnesia is reported to retard the reducibility of Ni by the formation of solid solution by Wurzler et.al [12] the correlation of dispersion with the specific BET surface area of the catalyst was plotted for catalysts that show >87% reducibility of Ni in Figure 38.

Figure 38 correlates Nickel metal area with BET-specific surface for catalysts with 7.5wt% Nickel and whose metal reducibility is better than 87%.

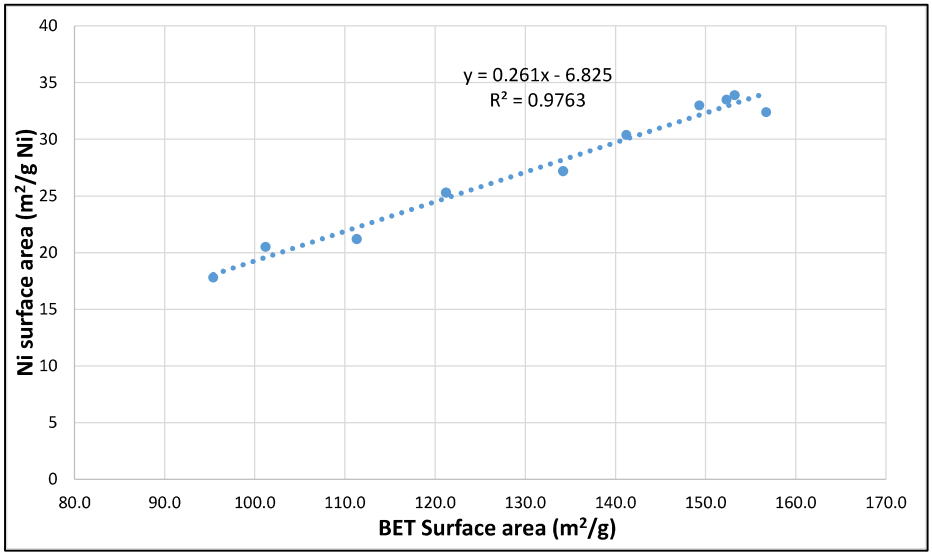

Figure 38: Correlation of Nickel metal area with BET surface area for catalysts with 7.5wt% and with Nickel reducibility >87%.

As seen in Figure 38 the correlation constant markedly improves from 0.534 to 0.976. Thus, it is clear that both BET surface area and degree of reducibility of Ni contribute to the surface area of Ni.

The regressed equation is:

Ni metal area (m^2/g) = 0.261 * BET specific surface area – 6.825 (Equation 3)
$R^2 = 0.976$

In view of the above the trend of Ni surface area was further examined by comparing specific Ni metal surface area with the degree of reducibility of NiO. This is shown in Figure 39 below.

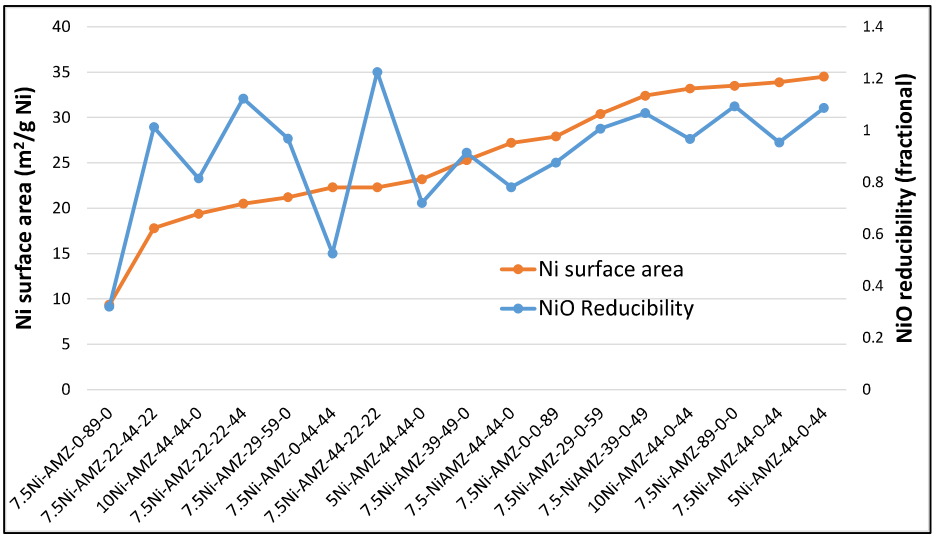

Figure 39: Trend of the specific surface area of Nickel metal with a degree of reducibility of NiO

As seen from trend in Figure 39 above, there is a reasonable qualitative trend of Ni metal surface area with degree of reducibility of NiO in the catalyst. It is notable that all the ternary Al-Zr catalysts which show close to complete reducibility of NiO show high dispersion (metal surface area) of Ni. These catalysts do not contain Mg as a component. In contrast all catalysts containing Mg (ternary Al-Mg and quaternary catalysts) show relatively low dispersion as determined by O_2 chemisorption. As seen in later sections, these catalysts show Ni particle size similar to ternary Al-Zr catalysts in HRTEM studies. Thus, it appears that the presence of Mg in these catalysts inhibits chemisorption of O_2 thus resulting in a lower value of calculated dispersion.

The trend of Ni metal surface area versus degree of Ni reducibility is regressed in Figure 40 below.

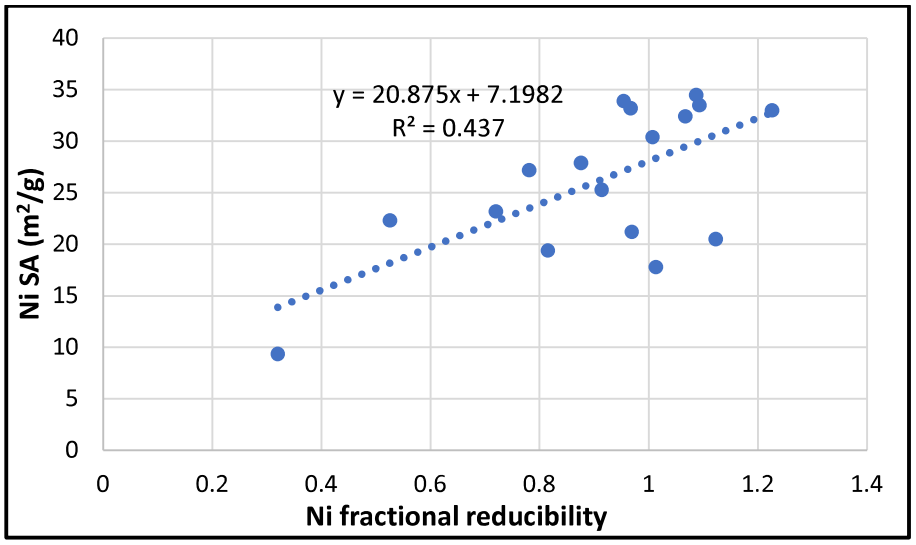

Figure 40: Trend of Nickel metal surface area versus the degree of Nickel reducibility

As seen from Figure 40, some of the catalysts which show high reducibility >0.9 also show high dispersion (data points above the regression line). These are exclusively those which do not contain Mg in the composition. Catalysts 7.5%Ni-AMZ-22-22-44 (quaternary catalyst containing Mg and is Zr rich), 7.5%Ni-AMZ-22-44-22 (Mg rich quaternary catalyst), 7.5%Ni-AMZ-29-59-0 (Mg rich ternary Al-Mg catalyst) have high reducibility but show poor dispersion (data points below the regression line). As mentioned above the reason appears to be a negative influence of Mg on chemisorption of O_2 on Ni in these catalysts.

Thus, based on trends of Figures 38, 39 and 40, it is clear that both BET surface area of the support and degree of reducibility of NiO affect the final dispersion of Nickel in the catalysts. To quantify the effect of both these parameters multiple regression of specific Nickel metal surface area as a function of these two parameters was carried out. The result of multiple regression for catalysts with 7.5wt% Nickel content and fractional reducibility > 0.87 is given below:

Specific Nickel metal surface area (m^2/g) = -9.728 + 0.2586 * BET surface area of the catalyst + 3.16 * fractional reducibility of NiO in the catalyst. (Equation 4)

Correlation constant for regression R^2 = 0.9803. Thus, the fit is very good.

However, the fit for multiple regression of BET-specific surface area and fractional reducibility of Nickel with Nickel surface area of the full data set is poor, indicating that both the metal reducibility and BET-specific surface area influence

Nickel surface area independently. The multiple regression equation for the full data set is:

Specific Nickel metal surface area (m^2/g) = 5.366 + 0.1107 * BET surface area of the catalyst + 8.207 * fractional reducibility of NiO in the catalyst. (Equation 5)
Correlation constant for regression R^2 = 0.6148.

3.7: XRD phase and crystallite size of the catalysts

The XRD phase and crystallite size of NiO was determined using a Bruker D8 FOCUS X-ray diffractometer with a Cu Kα source, wavelength 1.5406 Å. Samples were scanned in the 2-θ range of 5° to 80° at 0.04° per min rate and 0.25 step/s. The phase was identified by matching with a pattern from the in-built XRD library PDF-4. The crystallite size (CS) of different phases was determined from the most intense XRD peak using the Scherrer equation as mentioned below.

$$D=K\lambda/(\beta \cos \theta)$$

where D is the mean size of crystallites (nm), K is the crystallite shape factor, λ is the X-ray wavelength, B is the full width at half the maximum (FWHM) in radians of the X-ray diffraction peak and θ is the Braggs' angle (deg.)

The trend of crystallite size of NiO and BET-specific surface area with the composition of the support is shown in Figure 41 below.

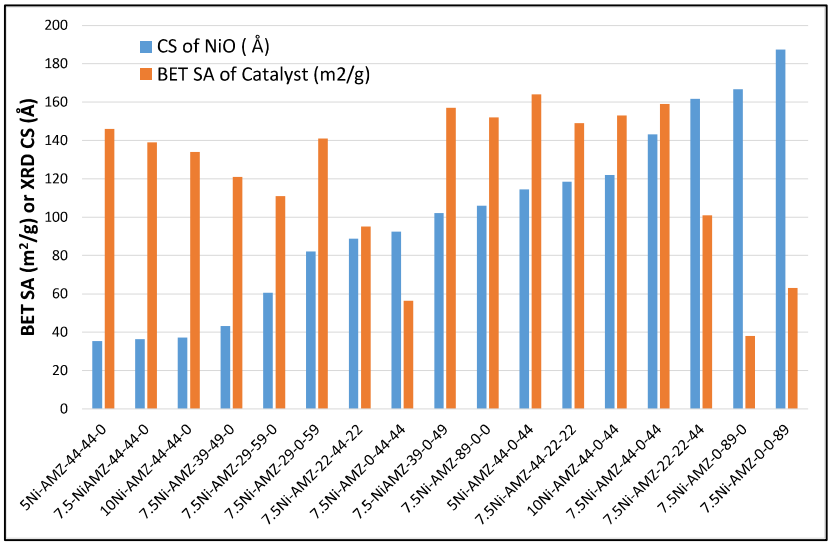

Figure 41: Trend of crystallite size of NiO and BET-specific surface area with the composition of the support

As seen in Figure 41, the trend of crystallite size of NiO in the binary catalysts is Al << Mg < Zr. There is an inverse correlation between the specific BET surface area of the catalyst and the XRD crystallite size for the binary catalysts which is as expected.

Amongst the ternary catalysts with 7.5wt% Nickel, the balanced alumina-magnesia catalysts show the smallest crystallite size. It is the smallest of all catalysts studied. This is followed by the alumina-magnesia catalysts with composition skewed in favor of magnesia. Crystallite size increases with increasing magnesia in the case of the catalysts with skewed composition. The trend is inversely related to BET surface area, as expected.

Next, come skewed alumina-zirconia catalysts with composition skewed in favor of zirconia. The balanced alumina-zirconia ternary catalysts show the highest crystallite size among the ternary catalysts. Crystallite size increases with decreasing zirconia in the case of the catalysts with skewed composition. There is no clear relation with BET surface area. The magnesia-zirconia catalyst falls in between the skewed alumina-zirconia series.

Navarro et.al [10] have studied M_xO_y-Al_2O_3 catalysts, where M= Zr, Ce, La or Mg, M/Al 0.035 (atomic) with 16-17 wt% NiO. They have reported a trend of Ni crystallite size after the reduction of the catalysts with H_2 at 650°C for 2 hours. The trend of crystallite size reported by them is Ni/Al-Zr > Ni/Al, Ni/Al-Ce, Ni/Al-Mg. Interestingly, the trend for NiO in the current study also shows a similar trend with ternary Al-Zr catalysts showing larger crystallite size than Al-Mg catalysts.

Bellido et.al. [17] have studied Ni/Y_2O_3-ZrO_2 catalysts prepared by polymerization of nitrates of all three components and impregnation of Ni on ceria-zirconia support. They report XRD crystallite size of NiO 125 Å -143 Å for the former and 259 Å for the latter catalysts. In comparison the binary 7.5%Ni-AMZ-0-0-89 binary Zr catalyst has a crystallite size 187 Å which is closer to the former catalysts reported by Bellido et.al.

The 7.5%Ni-AMZ-44-44-0 series shows a slight trend of increase in crystallite size with increasing Nickel content whereas the 7.5%Ni-AMZ-44-0-44 series does not show a clear trend between the 7.5wt% and 10wt% Nickel catalysts. The 5wt% Nickel catalyst shows the smallest crystallite size among the three.

The crystallite size of NiO in the quaternary catalysts increases in the order AMZ-22-44-22 < AMZ-44-22-22-<AMZ-22-22-44. Thus, quaternary catalysts rich in magnesia show the smallest crystallite size followed by catalysts rich in alumina and then zirconia. This trend is very different from that of binary catalysts. Hence, NiO appears to interact differently with the supports in these catalysts.

Between the series the magnesia and zirconia binary catalysts show the largest CS and the ternary alumina-magnesia catalysts with balanced composition show the smallest. The ternary Al-Mg catalysts (both balanced and skewed) show amongst the smallest CS across the entire set of catalysts. Ternary Al-Zr catalysts show CS of intermediate size. The skewed Al-Zr catalysts show smaller CS than the balanced catalyst which is opposite to the trend of ternary Al-Mg catalysts.

As seen in Figure 41, XRD crystallite size shows a limited correlation with BET-specific surface area. An inverse trend is observed for ternary catalysts comprising alumina-zirconia, and binary catalysts of magnesia or zirconia. The quaternary catalysts and ternary catalysts of balanced alumina-zirconia do not show a trend.

Similarly, a limited correlation is observed between XRD crystallite size and Ni reducibility or Ni dispersion. These Figures are shown in Appendix 9. Excepting for catalysts 7.5%Ni-AMZ-0-44-44, (ternary magnesia-zirconia), ternary alumina-zirconia catalysts with balanced composition, quaternary catalyst 7.5%Ni-AMZ-22-22-44 and binary catalysts of zirconia and magnesia, the remaining catalysts show a trend with the degree of Nickel reducibility. The correlation with Ni metal surface area is poorer than the correlation with the reducibility of Nickel. As expected, no correlation was observed with TEM particle size because the latter measures the size of clusters. The relation between XRD Crystallite size of NiO and median particle size determined by HRTEM is shown in Figure 42.

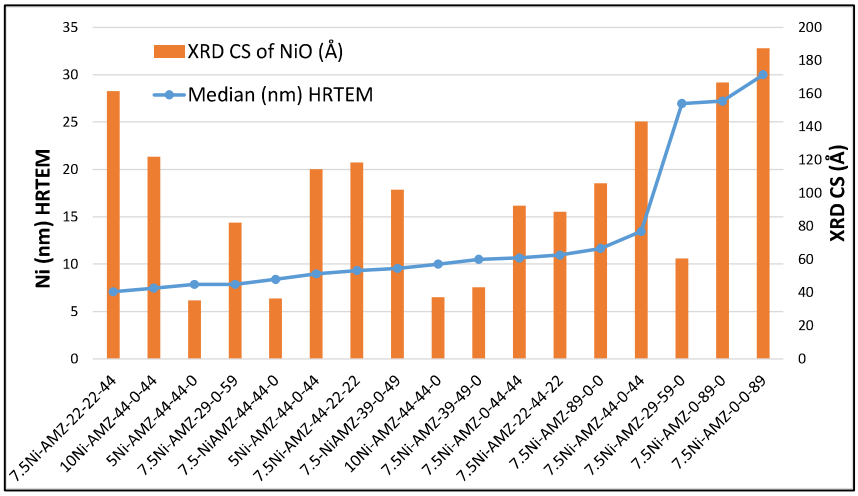

Figure 42: Relation between XRD CS of NiO and median particle size determined by HRTEM.

As seen from this Figure, there is a closer match between these parameters for binary Mg and Zr catalysts, ternary Al-Mg catalysts with balanced composition followed by ternary Al-Mg catalysts with composition skewed in favor of Mg. Ternary catalysts of Al and Zr and quaternary catalysts rich in Al or Zr show much higher XRD CS than particle size determined by HRTEM. This indicates they are composed of a significantly larger number of crystallites or grains.

The XRD pattern of the catalysts is shown in Appendix 8. As seen from these Figures most of the catalysts show a pattern similar to that of the support, which is used to prepare them, except for the presence of two peaks corresponding to NiO. The following catalysts show differences concerning the support:

1. 7.5%Ni-AMZ-89-0-0 (binary alumina) shows significantly higher crystallinity than its corresponding support 7.5%Ni-AMZ-89-0-0. The presence of NiO is observed.
2. 7.5%Ni-AMZ-0-89-0 (binary Magnesia) shows significant loss of crystallinity compared to its corresponding support AMZ-0-89-0. Peaks for MgO (Periclase) and NiO are present. A new peak at 67° 2θ is observed which could not be assigned (could be Ni-Mg solid solution). Peaks corresponding to Ni-Mg solid solution are present, which are also reported by Wurzler et.al.[12].
3. 7.5%Ni-AMZ-0-0-89 (binary zirconia) shows a tetragonal phase. Benito et.al [18] have studied Ni supported on monoclinic and tetragonal zirconia. They report that Ni supported on tetragonal zirconia exhibits better H_2 productivity.

4. 7.5%Ni-AMZ-0-44-44, which has a balanced composition of Mg and Zr, shows a significant loss of crystallinity of the t-ZrO_2 phase compared to its corresponding support AMZ-0-44-44. The peak for NiO is barely present.
5. All three catalysts with Ni varying from 5-7.5-10wt% Ni-AMZ-44-44-0 (ternary Al-Mg catalyst with balanced composition) show XRD patterns similar to the support AMZ-44-44-0. The NiO in these samples is masked/overlapped by the peak of $MgAl_2O_4$ (at 44.92° 2θ). Formation of MgAlO4 is also reported by Galetti et.al [9] who prepared the catalysts by coprecipitation, whereas Sanchez-Sanzhez et.al. [10] did not observe it nor periclase in case of catalysts prepared by impregnation of Mg nitrate on formed γ-Al2O3.
6. Similar to the ternary Al-Mg catalysts with balanced composition, the ternary Al-Mg catalysts with composition skewed in favor of Mg (7.5%Ni-AMZ-39-49-0 and 7.5%Ni-AMZ-29-59-0) also show XRD patterns similar to that of the support. NiO is masked/overlapped by the peak of $MgAl_2O_4$.
7. 7.5%Ni-AMZ-44-0-44 (ternary Al-Zr catalyst with balanced composition) shows significantly higher crystallinity than its corresponding support AMZ-44-0-44 whereas its counterparts with 5 and 10 wt% Ni show no significant difference in crystallinity relative to the support. The NiO in these samples is masked by the peak of $MgAl_2O_4$ (at 44.92° 2θ).
8. The Al-Zr catalysts with composition skewed in favor of Zr (7.5%Ni-AMZ-39-0-49 and 7.5%Ni-AMZ-29-0-59) do not show a significant difference in crystallinity from that of the support. Peaks of NiO are observed.
9. The three quaternary catalysts also do not show significant differences in crystallinity relative to their supports, except for the presence of peaks of NiO. The peak of NiO at 43.27° 2θ is clearly visible in 7.5%Ni-AMZ-44-22-22 (Al-rich quaternary catalyst) despite the presence of Mg, whereas it is masked by the peak of $MgAl_2O_4$ in the Mg and Zr rich catalysts.

3.8: High-Resolution Transmission Electron Microscopy (HRTEM) of calcined catalysts

The micrograph of binary Al catalyst 7.5%Ni-AMZ-89-0-0 is shown in Figure 43 below.

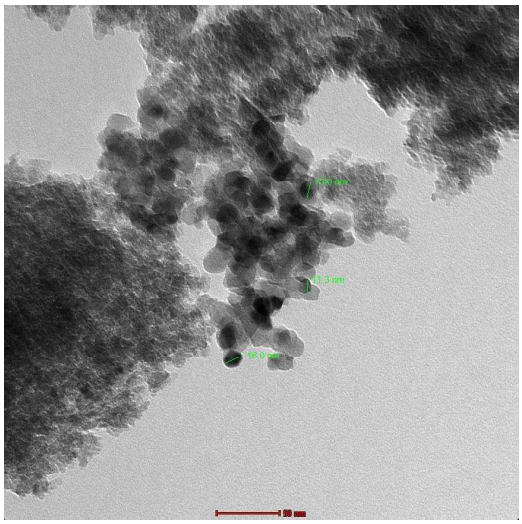

Figure 43: Micrograph of binary Al catalyst 7.5%Ni-AMZ-89-0-0

As seen from this Figure some regions are granular and others globular. XRD shows the presence of γ-Al_2O_3 and NiO phases. NiO is seen as dark-faceted particles. The median size of NiO particles is 11.6 nm and the average size is 13.2 nm. Lattice 'd' spacing 478 pm is observed.

A micrograph of binary Mg catalyst 7.5%Ni-AMZ-0-89-0 is shown in Figure 44 below.

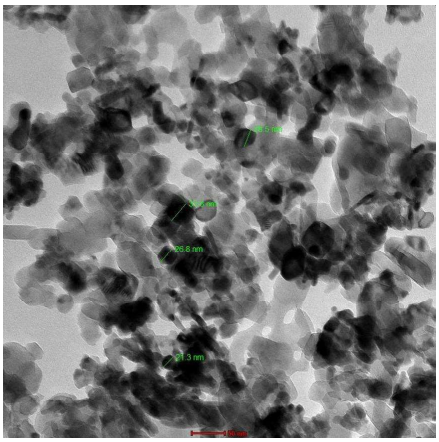

Figure 44: Micrograph of binary Mg catalyst 7.5%Ni-AMZ-0-89-0

As seen from the above Figure morphology is mainly faceted / globular particles with some lath-shaped ones. XRD shows the presence of periclase and NiO phases. Nickel is seen as dark faceted particles. The median size of NiO is 27.2 nm and the average is 26.1 nm. Lattice 'd' spacing not determined.

The micrograph of binary Zr catalyst 7.5%Ni-AMZ-0-0-89 is shown in Figure 45 below.

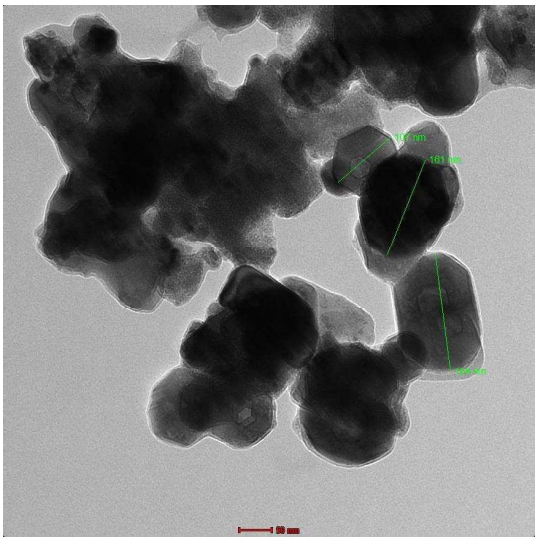

Figure 45: Micrograph of binary Zr catalyst 7.5%Ni-AMZ-0-0-89

As seen from above Figure dark blocky, hexagonal particles are observed. NiO particles range between 25-30 nm.

Thus, comparing the micrographs of the binary catalysts: Al-rich catalyst shows regions that are granular as well as globular whereas both the binary Mg and Zr catalysts show faceted particles without any granular morphology. The binary Al catalyst shows a significantly smaller particle size of NiO compared to the remaining two catalysts. This is attributed to its high BET-specific surface area compared to the latter.

The micrograph of ternary Al-Mg catalyst 7.5%Ni-AMZ-44-44-0 with a balanced composition of Al and Mg is shown in Figure 46 below.

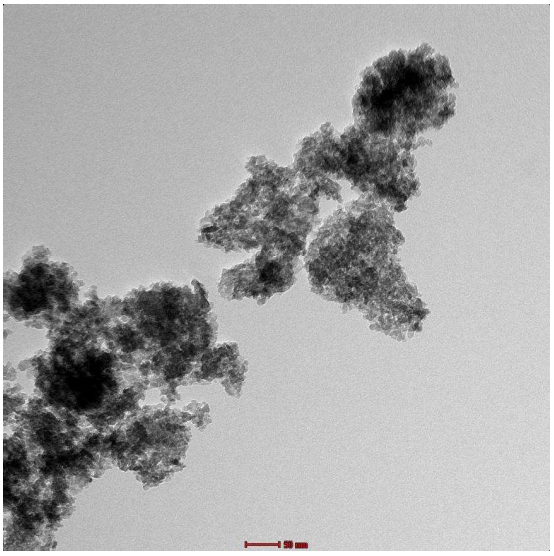

Figure 46: Micrograph of ternary Al-Mg catalyst 7.5%Ni-AMZ-44-44-0

As seen from the above figure combining Al and Mg leads to a uniform granular texture/morphology. This is attributed to the formation of the $MgAl_2O_4$ phase which is detected by XRD. TPR also supports this because the bimodal nature of peaks of Al and Mg change to unimodal (Appendix 7). NiO is seen as small dark particles embedded in the matrix. The size of NiO particles is a median of 8.39 nm and an average of 8.31 nm. Thus, a significant decrease in the size of NiO particles is observed relative to binary Mg catalyst. Particles with lattice 'd' spacing 552 and 559 pm are observed. Decreasing Ni content to 5wt% does not change the particle size of NiO (median 7.85 and average 8.57 nm). whereas increasing Ni to 10wt% increases the particle size of NiO to a median of 10 and an average of 11.3 nm.

Increasing Mg content to 49 wt% (7.5%Ni-AMZ-39-49-0) did not change the morphology/texture of the catalyst. Hence the figure is not shown here. It is included in Appendix 10. However, particle lattice 'd' spacing changes to 515 and 577 pm. The size of NiO particles increased to a median of 10.5 and an average of 10.2 nm.

Increasing Mg content still further to 59wt% (7.5%Ni-AMZ-29-59-0) changes the texture to granular (similar to binary Al) and globular faceted (similar to binary Mg) (Figure 47 below). Hence it appears that some Mg exists in MgO (periclase) phase which is also confirmed by XRD. Lattice ‘d’ spacing is 360

NiO is seen as dark-faceted particles in Figure 47 below. The particle size of NiO is a median of 26.9, with an average of 26.4 nm. Thus, particle size of NiO increases sharply and becomes comparable to that of binary Mg catalyst 7.5%Ni-AMZ-0-89-0.

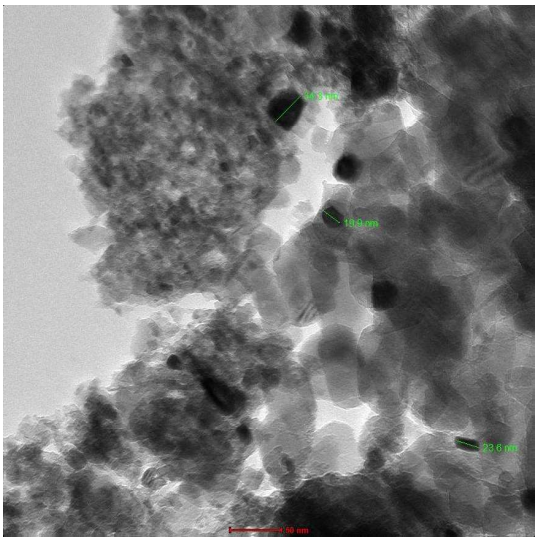

Figure 47: Micrograph of ternary Al-Mg catalyst 7.5%Ni-AMZ-29-59-0

As seen in Chapters 4 and 5 activity for ESR and EDR is significantly higher for binary Mg and ternary Al-Mg catalysts. The activity is compared with particle size of Ni (0) in the reduced catalysts there. Thus, particle size influences activity indicating that ESR and EDR are structure-sensitive reactions, as is also reported by R.Z.V van Meerten et.al [21] for methanation of CO on Nickel catalysts, Parlett et. al. [22] for ESR and Vogt et.al. [23] for dry and steam reforming of methane on Nickel catalysts.

A micrograph of ternary Al-Zr catalyst with balanced composition (7.5%Ni-AMZ-44-0-44) is shown in Figure 48 below.

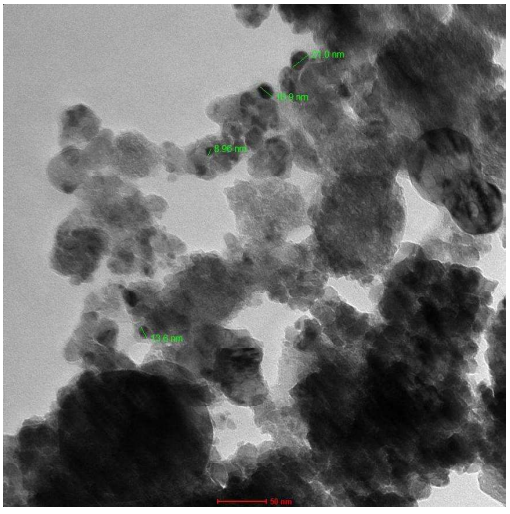

Figure 48: A micrograph of ternary Al-Zr catalyst with balanced composition (7.5%Ni-AMZ-44-0-44)

As seen from the Figure above, both granular and globular morphology along with strands of dark particles is observed in the matrix, which is similar to the binary

Al catalyst. Thus, it appears that at least some Al_2O_3 remains as such. Lattice 'd' spacing is 487 pm. NiO is observed as dark particles which are much smaller than the dark-colored ZrO_2 matrix particles. The size of NiO particles is a median 13.4 nm average of 13.9 nm. Thus, combining Al with Zr decreases the size of NiO significantly relative to the binary Zr catalyst. The particle size is in the same range as the binary Al catalyst.

Increasing ZrO_2 content to 49wt% (7.5%Ni-AMZ-39-0-49) changes the texture of the matrix (Figure 49 below). Fibrils are seen in the upper left-hand corner. Some granular texture with some faceted particles is also observed. Some linear strands of dark particles are also observed. This texture is significantly different from that of the ternary Al-Zr catalyst with a balanced composition. 7.5%Ni-AMZ-44-0-44. Lattice 'd' spacing is not measured.

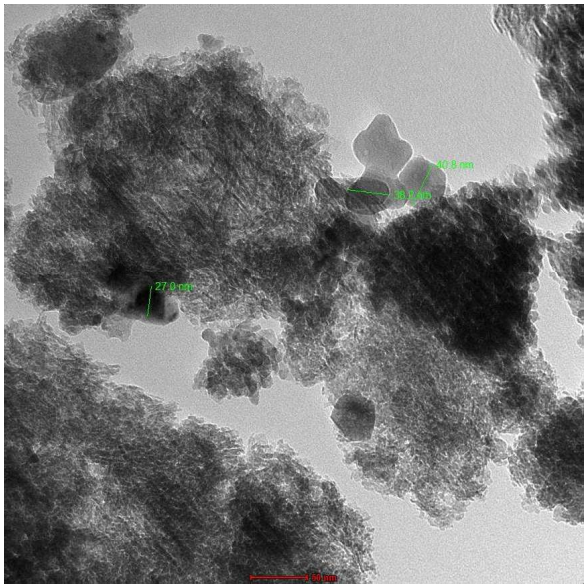

Figure 49: Micrograph of ternary Al-Zr catalyst with a balanced composition 7.5%Ni-AMZ-39-0-49

The median particle size of NiO is 9.55 nm and the average is 10.7 nm, which is smaller than that of 7.5%Ni-AMZ-44-0-44.

Increasing the ZrO_2 content to 59% (7.5%Ni-AMZ-29-0-59) changes the morphology to an irregular blocky texture. Granular or fibrillary morphology which is present in 7.5%Ni-AMZ-44-0-44 is very much diminished. Strands of dark particles remain (Figure 50 below).

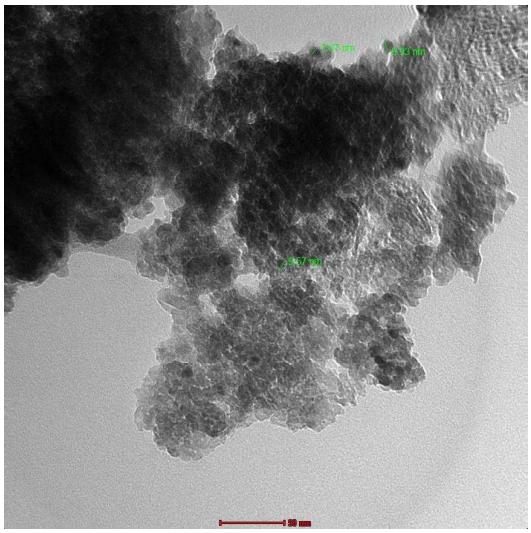

Figure 50: Micrograph of ternary Al-Zr catalyst with a balanced composition 7.5%Ni-AMZ-29-0-59

Thus, the strands of dark particles which appear in all three ternary Al-Zr catalysts appear to be characteristic of ternary Al-Zr catalysts. Lattice 'd' spacing is 465 pm. The size of NiO is a median of 7.8 nm and an average of 8.3 nm, which has decreased still further with increasing ZrO_2 content. This is different from the behavior of ternary Al-Mg catalysts where the size of NiO increases with increasing MgO content. The reason could be an increase in zirconia alumina solid solution with increasing zirconia content.

The micrograph of the ternary Mg-Zr catalyst is shown in Figure 51 below.

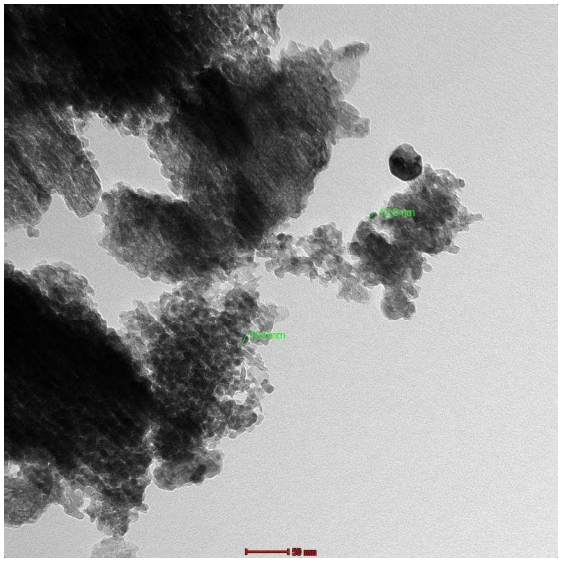

Figure 51: Micrograph of ternary Mg-Zr catalyst with a balanced composition 7.5%Ni-AMZ-0-44-44

As seen from this Figure linear dark strands which are also observed in ternary Al-Zr catalysts are conspicuously present. Globular morphology of binary Mg catalysts is also present. Lattice 'd' spacing is 438 pm. NiO is seen as dark particles embedded in the matrix. Its size is a median of 10.6 and an average of 10.0 which is in between binary Al and ternary Al-Mg or Al-Zr catalysts.

The micrograph of the quaternary Al-rich catalyst 7.5%Ni-AMZ-44-22-22 is shown in Figure 52 below. The morphology is similar to that of ternary Al-Mg (globular) and ternary Al-Zr catalysts (linear dark strands). The granular texture of binary Al is barely present. XRD also shows an amorphous phase indicating that Al could be present in the form of a solid solution with Zr and as $MgAl_2O_4$. Lattice 'd' spacing is 430 pm and 544 pm. The size of NiO is median 9.3 average 9.08 nm which is in the same range as ternary Al-Zr catalysts.

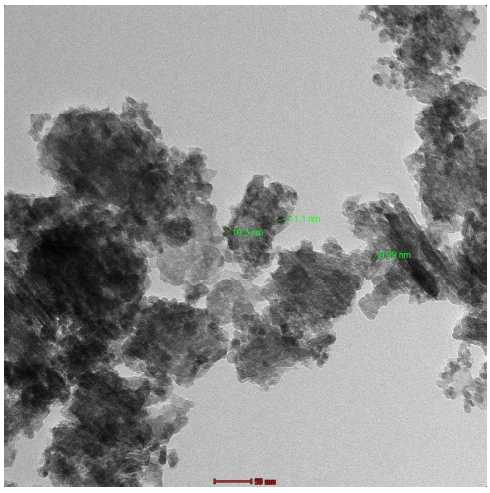

Figure 52: Micrograph of the quaternary Al-rich catalyst 7.5%Ni-AMZ-44-22-22

Increasing MgO at the expense of Al_2O_3 (Mg-rich quaternary catalyst 7.5%Ni-AMZ-22-44-22) shifts the texture closer to that of ternary Al-Mg catalyst (7.5%Ni-AMZ-44-44-0). (Refer Appendix 10). Lattice 'd' spacing is 430 and 548 nm. The size of NiO particles is a median 10.9 nm average of 12.8 nm, which is larger than that of the quaternary Al-rich catalyst.

Increasing ZrO_2 at the expense of Al_2O_3 (Zr-rich quaternary catalyst 7.5%Ni-AMZ-22-22-44) shifts the texture towards that of ternary Al-Zr catalyst 7.5%Ni-AMZ-44-0-44). The fraction of linear strands of dark particles increases. (Refer Appendix 10). The lattice 'd' spacing is 465 nm. The size of NiO particles is a median 7.1 nm average of 8.2 nm, which is the smallest amongst the quaternary catalysts.

3.9: High-Resolution Transmission Electron Microscopy (HRTEM) of reduced and stabilized supported Ni catalysts

The micrographs of HRTEM of select supported Ni catalysts are shown in Appendix 11. These are 7.5%Ni-AMZ-0-89-0, 7.5%Ni-AMZ-0-0-89, 7.5%Ni-AMZ-44-44-0, 7.5%Ni-AMZ-0-44-44, 7.5%Ni-AMZ-44-0-44 and 7.5%Ni-AMZ-22-44-22, These catalysts were subjected to TPR up to 550°C and cooled in flowing N_2 to ambient temperature prior discharge from the reactor. The particle size of Ni was measured. Lattice 'd' spacing of multiple particles was also measured by the CCD technique. The results show that:

1. Ni particles are faceted in all cases.
2. Ni particles range in size 8-12 nm (7.5%Ni-AMZ-0-0-89, 7.5%Ni-AMZ-0-89-0, 7.5%Ni-AMZ-44-0-44, 7.5%Ni-AMZ-44-44-0). Some larger agglomerates of Ni are also observed but they are fewer than for other catalysts listed below.
3. 7.5%Ni-AMZ-0-44-44 and quaternary 7.5%Ni-AMZ-22-44-22 show relatively larger Ni particles
4. The significant decrease observed in the size of Ni particles relative to that of the corresponding NiO particles from which they formed by chemical reduction indicates that Ni redisperses during reduction. Similar results are reported by Phichitul et.al. [23] and Nakayama et.al [24]. The reason for this is explained in sections immediately below.
5. The results of lattice 'd' spacing indicate the following:
    i. Lattice 'd' spacing 2.38-2.41 Å is present in all the catalysts and corresponds to NiO (1,1,1) which is as expected.
    ii. Lattice 'd' spacing 2.43 Å is observed in 7.5%Ni-AMZ-0-89-0, 7.5%Ni-AMZ-44-0-44, 7.5%Ni-AMZ-44-44-0, 7.5%Ni-AMZ-0-44-44 and 7.5%Ni-AMZ-22-44-22. This value is characteristic of MgO (1,1,1), $MgAl_2O_4$ (3,1,1) and Ni-aluminate (3,1,1). Combining these results with those of XRD it is clear that MgO (Periclase) is present in 0-89-0, whereas $MgAl_2O_4$ is present in ternary catalysts containing both alumina and magnesia (7.5%Ni-AMZ-44-44-0 and 7.5%Ni-AMZ-22-44-22). The particles in 44-0-44 would be Ni-aluminate.

iii. Catalysts containing Zr show lattice ‘d’ spacing 2.52-2.55 Å which is assigned to ZrO_2 (1,1,1)

iv. La_2O_3 (0,0,2) and CeO_2 (1,1,1) were identified in catalysts 7.5%Ni-AMZ-0-44-0 and 7.5%Ni-AMZ-0-0-89 respectively was identified through particles with 'd' spacing 3.06 Å and 3.15 Å respectively.

v. All catalysts containing Mg show particles with a 'd' spacing of 2.21 Å. This could not be assigned. It may be Ni-Mg solid solution.

vi. Similarly, the binary and ternary catalysts containing zirconium or a combination of Zr and Al show particles with a 'd' spacing of 2.47 Å. This too could not be assigned.

vii. Lattice 'd' spacing values 2.63 Å (7.5%Ni-AMZ-0-89-0, 7.5%Ni-AMZ-22-44-22 both catalysts containing Mg), 2.47-2.48 Å (7.5%Ni-AMZ-0-0-89, 7.5%Ni-AMZ-44-0-44 and 7.5%Ni-AMZ-22-44-22 all three containing Zr), 2.59-2.60 (7.5%Ni-AMZ-0-89-0, 7.5%Ni-AMZ-44-44-0 Mg containing), 2.63 Å (7.5%Ni-AMZ-0-89-0, 7.5%Ni-AMZ-22-44-22 Mg containing), 2.65-2.67 Å (7.5%Ni-AMZ-44-44-0, 7.5%Ni-AMZ-0-44-44), 2.77 Å (7.5%Ni-AMZ-0-44-44, 7.5%Ni-AMZ-22-44-22), 2.97 Å (7.5%Ni-AMZ-0-89-0, 7.5%Ni-AMZ-44-44-0), 3.21 Å (7.5%Ni-AMZ-0-44-44), 3.53 Å (7.5%Ni-AMZ-44-44-0) could not be assigned. However, the presence of these particles indicates the possibility of interactions between the various phases of the support as well as the interaction of Ni with these phases.

The particle size of NiO in calcined catalysts is compared with that of Ni(0) in the corresponding reduced catalyst in Table 3 below. Peak temperature of reduction in TPR is also included.

Table 3: Particle Size of NiO of Calcined Catalyst and of Ni (0) of Reduced & Stabilized Catalyst

Sr. No.	Catalyst	Peak Temperature of Reduction (^oC) in TPR	Reduced & Stabilized catalyst Median size Ni(0) (nm)	Calcined oxide form of catalyst. Median Size of NiO (nm)
1	7.5%Ni-AMZ-0-0-89	448°C	10.3	30
2	7.5%Ni-AMZ-0-89-0	464°C	9.9	27.2
3	7.5%Ni-AMZ-44-0-44	535°C	10.7	13.5

4	7.5%Ni-AMZ-44-44-0	580°C	9.2	8.4
5	7.5%Ni-AMZ-39-49-0	568°C	10.3	10.5
6	7.5%Ni-AMZ-29-59-0	563°C	12.4	26.9
7	7.5%Ni-AMZ-0-44-44	762°C	14	10.6
8	7.5%Ni-AMZ-22-44-22	731°C	13.3	10.9

The following observations are made from Table 3 above:

1. The particle size of NiO decreases significantly in binary Mg or Zr catalysts and ternary Al-Mg catalyst which is rich in Mg when these catalysts are reduced to form Ni(0). It is noted that all these catalysts present a reduction of NiO at a temperature lower than 563°C. The melting point of Ni is 1455°C and its Huttig temperature is 518K (245°C) and Tammann temperature is 863K (590°C). As per reference Argyl and Bartholomew [24] Tammann temperature is the temperature for the onset of mobility of atoms from the bulk crystal lattice, whereas Huttig temperature is the temperature of onset of surface mobility of atoms. The former is well below the reduction temperature (550°C) and the latter close to the reduction temperature. Similar behavior of decrease in particle size upon reduction of NiO is reported by C. Phichitkul [25]. The author attributes this behavior to the fracture of NiO particles during its reduction, which causes redispersion. The reason is attributed to a 40% decrease in volume during reduction which causes tensile stress on Ni and compressive stress on the support. T. Nakayama et.al. [26]
2. Frusteri et.al. [27] have studied K promoted Ni impregnated on MgO. They report Ni(0) particle size about 7.9 nm for the freshly reduced un-promoted catalyst. These are close to 9.2 nm observed for balanced Al-Mg catalysts (9.2 nm) in the current study.
3. Shuirong Li et.al [7] have studied NiO supported on ZrO_2. They report particle size of Ni(0) 23.7 nm. Unfortunately, the particle size of Ni(0) was not determined in binary ZrO_2 catalyst in the current study. However, results of ESR in chapter 4 show that this catalyst has poor activity, which indirectly indicates poor dispersion.
4. Introduction of Al along with Mg or Zr in ternary catalysts 7.5%Ni-AMZ-44-44-0 or 7.5%Ni-AMZ-44-0-44 respectively decreases the

particle size of NiO significantly relative to the binary catalysts of Mg or Zr. However, as seen from the results of Ni(0) particle size of catalysts after use for ESR (Table 7 chapter 4), only the ternary Al-Zr catalysts show resistance to sintering whereas the ternary Al-Mg catalysts do not. Ji Hwan Song et.al. [28] have studied 15%Ni-6%Sr-Al_2O_3-ZrO_2 xerogel catalysts prepared by epoxide driven sol-gel method. They report average particle size of Ni(0) 10 nm which is close to that of ternary Al-Zr catalysts achieved in the current study (10.7 nm).

3. Similar to ternary Al-Zr catalysts, all the quaternary catalysts do not show significant changes in particle size after reduction. They too show good resistance to sintering during use for ESR as shown in Chapter 4.

4. Particle size of NiO increases exponentially with the Mg content of ternary Al-Mg catalysts.

3.10: Conclusions

Seventeen supported metal catalysts are prepared by incipient wetness impregnation. These comprise Ni supported on supports of binary, ternary and quaternary compositions of oxides of Al, Mg and Zr which also contain a fixed quantity of lanthana and ceria. Ni content is varied in select ternary supports comprising Al-Mg or Al-Zr. The content of La_2O_3 and CeO_2 is constant at nominal 5.4wt% each across all the catalysts. They are thoroughly characterized by routine and advanced characterization techniques. Their characteristics are correlated with trends of ESR and EDR in chapters 4 and 5.

The trend of specific surface area and pore volume of the supported catalysts remain largely unchanged concerning that of the supports. There is a linear decrease in both specific surface area and pore volume with an increase in the Ni content of the catalyst. This is in line with expectations for catalysts prepared by impregnation.

Acidity measurements by ammonia TPD show that Nickel contributes to the Lewis acidity of the supports. This changes the trend of acidity of support due to the contribution of Lewis acidity from Nickel. Supporting nickel appears to decrease strong acidity in supports that contain zirconia and increase strong acidity in most of the supports which contain magnesia. A similar trend is observed for total acidity.

The reducibility of Ni studied by H_2-TPR shows clear trends of changes in metal support interaction with the composition of the catalyst. Nickel oxide reduces relatively easily (at lower temperatures) on binary Zr and ternary Al-Zr supports indicating weak interaction with NiO. The high-temperature peak for the reduction of NiO is not observed in these catalysts. Whereas, both low and high-temperature peaks are observed on the binary Al and Mg supports. Ternary Al-Mg and all three quaternary supports show high-temperature peaks indicating strong interaction with NiO. However, particle size of Ni after use for ESR or EDR shows lesser sintering of Ni(0) in catalysts containing Zr. Thus, the strength of the interaction of NiO with support does not correlate with resistance to the sintering of the metallic phase Ni(0). Changes from bimodal to unimodal peaks of reduction of NiO indicate changes in the composition of support such as the formation of solid solution which in turn changes their interaction with NiO (relative to corresponding mono-component supports).

Ni supported on binary Mg and ternary catalysts containing Mg shows low reducibility of NiO which is attributed to the formation of solid solution of Ni with Mg. However, this appears to increase inherent catalyst activity as observed from the conversion of ethanol in ESR and EDR runs (in chapters 4 and 5). The XRD pattern of the binary Mg catalyst shows peaks that are significantly different from those of MgO and NiO, supporting the formation of their solid solution.

Catalysts based on supports containing Mg show significantly lower dispersion of Ni (0) as determined by O_2 titration. On the other hand, catalysts based on supports that contain zirconia show high dispersion of Ni (0). Thus, dispersion correlates with ease of reducibility of NiO. However, the particle size of Ni(0) in catalysts containing Mg (as determined by HRTEM) is not significantly different from that of other catalysts. It shows Ni(0) particles which are similar in size to the other catalysts. Thus, while the amount of dispersed Ni(0) is lower in catalysts that contain Mg, particle size is comparable to other catalysts.

The dispersion of Ni correlates well with specific BET surface area and degree of reducibility of Ni. An especially good fit is observed when the specific surface area is normalized for that required to form a monolayer of NiO on the surface of the support.

XRD crystallite size of NiO is significantly smaller for ternary supports of Al-Mg and Mg-rich quaternary catalysts, than Al-Zr or Zr-rich quaternary catalysts. The

particle size of NiO determined by HRTEM also supports this observation. Conversion of ethanol in ESR and EDR is also higher for these catalysts compared to catalysts containing Zr. Results of XRD show that alumina, magnesia, and zirconia exist as γ-Al_2O_3, periclase or t-ZrO_2 in binary catalysts whereas they form $MgAl_2O_4$ or zirconia-alumina solid solution in the ternary and quaternary catalysts.

Supporting Ni onto the supports does not change the XRD pattern for the majority of the catalysts. However, an increase in crystallinity is observed for 7.5% AMZ-89-0-0 and 7.5%Ni-AMZ-44-0-44. Whereas binary Mg (7.5%Ni-AMZ-0-89-0) shows a complete change in the XRD pattern which is attributed to the formation of Ni-Mg solid solution. Crystallinity loss is also observed in ternary Mg-Zr catalyst 7.5%Ni-AMZ-0-44-44. However, this catalyst shows relatively poor activity in ESR and EDR.

HRTEM of calcined catalysts shows distinct differences in morphology based on the presence of Al, Mg or Zr in binary catalysts. These distinctions diminish in ternary and quaternary catalysts indicating reactivity between these components. Binary magnesia 7.5%Ni-AMZ-0-89 and binary zirconia 7.5%Ni-AMZ-0-0-89 show significantly larger particles of NiO which are attributed to their low specific BET surface area. Incorporating Al along with Mg or Zr increases specific BET surface area which results in better dispersion of NiO (smaller particle size). However, increasing the Mg content of support in ternary Al-Mg catalysts increases the particle size of supported NiO.

HRTEM of reduced and stabilized catalysts shows faceted Ni particles. The particle size is relatively larger for ternary Mg-Zr (7.5%Ni-AMZ-0-44-44) and quaternary Mg-rich catalyst (7.5%Ni-AMZ-22-44-22). Lattice 'd' spacing showed the presence of some phases which are expected and also a good number of particles with d spacing that could not be assigned. The latter indicates interaction between components of the support by way of the formation of solid solutions. The particle size of NiO decreases significantly upon reduction in binary Mg (7.5%Ni-AMZ-0-89-0), Zr (7.5%Ni-AMZ-0-0-89) or ternary Al-Mg (7.5%Ni-AMZ-29-59-0) catalysts indicating redispersion of Ni as it forms from the reduction of NiO. Ternary Al-Zr and quaternary catalysts do not show a significant decrease in particle size upon reduction of NiO to Ni(0). These catalysts show better resistance to sintering than the Al-Mg catalysts in ESR and EDR of ethanol as shown in subsequent chapters.

References:

1. Ashutosh Kumar, R. Prasad and Y.C. Sharma; Steam Reforming of ethanol: Production of renewable hydrogen; International Journal of Environmental Research and Development; 4(2), 2014; 203-212.
2. Meng Ni, Dennis Y.C. Leung, Michael K.H. Leung; A review on reforming bioethanol for hydrogen production; International Journal of Hydrogen Energy; 32 (2007); 3238-3247.
3. J.L. Contreras, J. Salmones, J.A. Colín-Luna, L. Nuño, B. Quintana, I. Córdova, B. Zeifert, C. Tapia, G.A. Fuentes ; Catalysts for H_2 production using ethanol steam reforming (a review); International Journal of Hydrogen Energy; 39 (2014); 18835-18853.
4. Zahira Yaakob, Ahmed Bshish, Ali Ebshish, Siti Masrinda Tasirin, and Fatah H. Alhasan; Hydrogen production by steam reforming of ethanol over nickel catalysts supported on sol gel made alumina: influence of calcination temperature on supports; Materials; 6 (2013); 2229-2239.
5. F. Frusteri, S. Freni, V. Chiodo, S. Donato, G. Bonura, S. Cavallaro; Steam and auto-thermal reforming of bioethanol over MgO and Ni supported catalysts; International Journal of Hydrogen Energy; 3, (2006); 2193-2199.
6. Prakash Biswas and Deepak Kunzru; Steam reforming of ethanol for the production of hydrogen over Ni/CeO_2-ZrO_2 catalyst: Effect of support and metal loading; International Journal of Hydrogen Energy; 32 (2007); 969-980.
7. Shuirong Li, Chengxi Zhang, Zhiqi Huang, Gaowei Wua and Jinlong Gong; A Ni@ZrO2 nanocomposite for ethanol steam reforming: enhanced stability vis strong metal-oxide interaction; Chemical Communication; 49 (2013); 4226.
8. Seung Ju Han, Yongju Bang, Jeong Gil Seo, Jaekyeong Yoo, In Kyu Song, International Journal of Hydrogen Energy; 38 (2013); 1376-1383.
9. Agustin E. Galetti, Marianna N. Barroso, Manuel F. Gomez, Luis A, Arrua, Antonia Monzon, M. Cristina Abello; Promotion of Ni/MgAl2O4 catalysts with rare earth for the ethanol steam reforming reaction, Catalysis Letters; 142 (2012); 1461-1469.
10. M.C. Sanchez-Sanchez, R.M. Navarro, J.L.G. Fierro; Ethanol steam reforming over Ni/M_xO_y-Al_2O_3 (M=Ce, La, Zr, Mg) catalysts: Influence of

support on the hydrogen production; International Journal of Hydrogen Energy; 32 (2007); 1462-1471.

11. Feifei Yang, Danwei Liu, Yuntao Zhao, Hua Wang, Jinyu Han, Q. Ge, Xinli Zhu; "Size Dependence of Vapor Phase Hydrodeoxygenation of m -Cresol on Ni/SiO_2 Catalysts," ACS Catalysis; 8 (3), (2018); 1672–1682.
12. Gleicielle T. Wurzler, Raimundo C. Rabelo-Neto, Lisiane V. Mattos, Marco A. Fraga, Fabio B. Noronha; Steam reforming of ethanol for hydrogen production over MgO-supported Ni-based catalysts; Applied Catalysis A: General; 518 (2016); 115-128.
13. Fabien Aupretre, Claude Descorme, Daniel Duprez, Dominique Casanave, Denis Uzio; Ethanol steam reforming over $Mg_xNi_{1-x}Al_2O_3$ spinel oxide-supported Rh catalysts; Journal of Catalysis; 233(2), (2005); 464-477.
14. Alberto M. Becerra, Adolfo E. Castro; An investigation on the presence of $NiAl_2O_4$ in a stable Ni on alumina catalyst for dry reforming; Journal of the Chilean Chemical Society; 50 (2); (2005); 465-469.
15. Raúl Carrera Cerritos, Rosalba Fuentes Ramírez, Alberto F. Aguilera Alvarado, J. Merced Martínez Rosales, Tomás Viveros García, and Ignacio R. Galindo Esquivel; Steam reforming of ethanol over Ni/Al_2O_3-La_2O_3 catalysts synthesized by sol-gel; Industrial. Engineering and Chemical Research.; 50 (2011); 2576-2584.
16. Xiaoyong Wang, Biying Zhao, De-en Jiang, Youchang Xie; Monolayer dispersion of MoO_3, NiO and their precursors on γ-Al_2O_3; Applied Catalysis. A: General; 188 (1999); 201-209.
17. Jorge D.A. Bellido, Eurico Y. Tanabe, Elisabete M. Assaf; Carbon dioxide reforming of ethanol over Ni/Y_2O_3-ZrO_2 catalysts; Applied Catalysis B: Environmental; 90 (2009); 485-488.
18. M. Benito, R. Padilla, L. Rodríguez, J.L. Sanz, L. Daza; Zirconia supported catalysts for bioethanol steam reforming: Effect of active phase and zirconia structure; Journal of Power Sources; 169 (2007); 167-176.
19. Tatiana de Freitas Silva, Joelmir Augusto Costa Dias, Cristhiane Guimarães Maciela and José Mansur Assafa; Ni/Al_2O_3 catalysts: effects of the promoters Ce, La and Zr on the methane steam and oxidative reforming reactions; Catalysis Science and Technology; 3 (2013); 635.

20. Paula Osorio-Vargas, Nicolás A. Flores-González, Rufino M. Navarro, Jose L.G. Fierro, Cristian H. Campos, Patricio Reyes; Improved stability of Ni/Al_2O_3 catalysts by effect of promoters (La_2O_3, CeO_2) for ethanol steam-reforming reaction; Catalysis Today; 259 (2015); 27-38.
21. R.Z.C. van Meerten, A.H.G.M. Beaumont, P.F.M.T. van Nisselrooij, J.W.E. Coenen; Structure sensitivity and crystallite size change of Ni during methanation of CO/H_2 on nickel-silica catalysts; Surface Science; 135 (1-2), (1983); 565-579.
22. Christopher M.A. Parlett, Ayse Aydin, Lee J. Durndell, Lucia Frattini, Mark A. Isaacs, Adam F. Lee, Xiaotong Liu, Luca Olivi, Rima Trofimovaite, Karen Wilson, Chunfei Wu; Tailored mesoporous silica supports for Ni catalyzed hydrogen production from ethanol steam reforming, Catalysis Communications; 91 (2017); 76-79.
23. Charlotte Vogt, Jelle Kranenborg, Matteo Monai, and Bert M. Weckhuysen; Structure sensitivity in Steam and Dry methane reforming over Nickel: Activity and Carbon formation; ACS Catalysis; 10 (2020); 1428-1438.
24. Morris D. Argyle and Calvin H. Bartholomew; Heterogeneous deactivation and regeneration: A review; Catalysts; 5 (2015); 145-269.
25. C. Phichitkul; Catalyst activity and deactivation mechanism of supported NiO in CH_4 oxidation; Ph.D. Thesis; 1981, California Institute of Technology and Engineering.
26. Tetsunori Nakayama, Masahiko Arai, Yoshiyuki Nishiyama; Dispersion of Nickel particles supported on alumina and silica in Oxygen and Hydrogen; Journal of Catalysis; 87(1) (1984); 108-115.
27. F. Frusteri, S. Freni, V. Chiodo, L. Spadaro, G. Bonura, S. Cavallaro; Potassium improved stability of Ni/MgO in the team reforming of ethanol for the production of hydrogen for MCFC; Journal of Power Sources; 132 (2004); 139-144.
28. Ji Hwan Song, Seung Ju Han, Jaekyeong Yoo, Seungwon Park, Do Heui Kim, In Kyu Song; Hydrogen production by steam reforming of ethanol over Ni-Sr-Al_2O_3-ZrO_2 aerogel catalyst; Journal of Molecular Catalysis A: Chemical; 424(2016); 342-350.